

PRO-VPT: Distribution-Adaptive Visual Prompt Tuning via Prompt Relocation

Chikai Shang^{1,2} Mengke Li^{3,5} Yiqun Zhang^{4,5} Zhen Chen⁶ Jinlin Wu^{6,7}
 Fangqing Gu^{4,5*} Yang Lu^{1,2,5*} Yiu-ming Cheung⁵

¹Key Laboratory of Multimedia Trusted Perception and Efficient Computing, Ministry of Education of China, Xiamen University

²School of Informatics, Xiamen University ³Shenzhen University ⁴Guangdong University of Technology

⁵Hong Kong Baptist University ⁶CAIR, HKISI, CAS ⁷MAIS, CASIA

ckshang12@gmail.com fqgu@gdut.edu.cn luyang@xmu.edu.cn

Abstract

Visual prompt tuning (VPT), i.e., fine-tuning some lightweight prompt tokens, provides an efficient and effective approach for adapting pre-trained models to various downstream tasks. However, most prior art indiscriminately uses a **fixed** prompt distribution across different tasks, neglecting the importance of each block varying depending on the task. In this paper, we introduce adaptive distribution optimization (ADO) by tackling two key questions: ① How to appropriately and formally define ADO, and ② How to design an adaptive distribution strategy guided by this definition? Through empirical analysis, we first confirm that properly adjusting the distribution significantly improves VPT performance, and further uncover a key insight that a nested relationship exists between ADO and VPT. Based on these findings, we propose a new VPT framework, termed **PRO-VPT** (iterative Prompt RelOcation-based VPT), which adaptively adjusts the distribution built upon a nested optimization formulation. Specifically, we develop a prompt relocation strategy derived from this formulation, comprising two steps: pruning idle prompts from prompt-saturated blocks, followed by allocating these prompts to the most prompt-needed blocks. By iteratively performing prompt relocation and VPT, our proposal can adaptively learn the optimal prompt distribution in a nested optimization-based manner, thereby unlocking the full potential of VPT. Extensive experiments demonstrate that our proposal significantly outperforms advanced VPT methods, e.g., PRO-VPT surpasses VPT by 1.6 pp and 2.0 pp average accuracy, leading prompt-based methods to state-of-the-art performance on VTAB-1k and FGVC benchmarks. The code is available at <https://github.com/ckshang/PRO-VPT>.

1. Introduction

Fine-tuning pre-trained vision models (PVMs) [26] has proven remarkably effective in adapting to a variety of

*Corresponding authors.

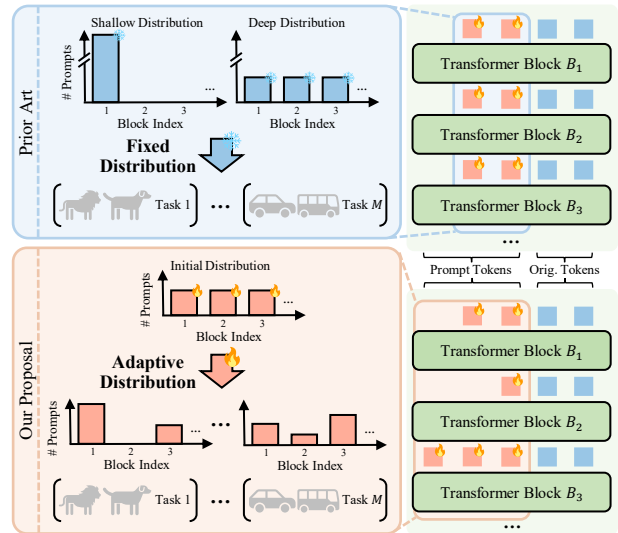


Figure 1. **PRO-VPT (ours) vs. prior art in VPT.** Existing VPT approaches typically insert trainable prompts into the PVM with a pre-specific static distribution, whether shallow or deep, and optimize these prompts to drive the PVM to conduct downstream tasks. Compared to the prior art, our proposal (PRO-VPT) adaptively adjusts prompt distribution by treating it as an optimization objective and coupling the distribution optimization with prompt tuning.

downstream tasks [14, 30, 65]. However, the computational and storage costs associated with full fine-tuning are prohibitively high, particularly as model sizes continue to grow [1, 40, 57]. To overcome these challenges, parameter-efficient fine-tuning (PEFT) methods [2, 20, 61, 62], such as visual prompt tuning (VPT) [22], have emerged as more promising alternatives, garnering significant attention.

Instead of updating all model parameters directly, VPT inserts lightweight learnable prompt tokens into the input space of Transformer blocks, with either a shallow distribution (inserted only in the first block) or a deep distribution (uniformly inserted across all blocks), while keeping the PVM frozen. This approach significantly reduces the number of parameters that need to be fine-tuned, thereby lowering the computational and memory overhead [14]. Follow-up

research further enhances this pipeline by improving aspects such as prompting architecture [13, 50, 52], prompt initialization [58], and prompt propagation structure [5, 63, 71].

Despite these advancements, most of the prior art still relies on a preset fixed prompt distribution, either shallow or deep, across various downstream tasks, as illustrated in Fig. 1. However, recent findings reveal that the importance of each pre-trained block varies significantly across different tasks [12, 28, 43, 49, 60], underscoring the need to dynamically tailor the fine-tuning intensity for each block to improve task performance [11, 25, 29, 45, 53]. This implies that indiscriminately using a fixed prompt distribution may not fully exploit the potential of VPT, motivating us to adaptively adjust the distribution to better accommodate each task.

In this paper, we naturally consider prompt distribution as one of the optimization objectives, which we refer to as adaptive distribution optimization (ADO). As the focus pivots towards the ADO problem, new questions arise. **First**, since the underlying nature of distribution optimization is still unexplored, the definition of ADO remains unclear. For instance, defining it as a one-shot process or an iterative one leads to a critical consideration, namely whether the effectiveness of distribution adjustments is influenced by ongoing prompt updates. This leads us to our first key question: ① *How can we appropriately and formally define ADO?* (§ 3.2) **Second**, once the definition of ADO is established, a more essential question emerges: ② *How can we achieve adaptive distribution derived from this definition?* (§ 3.3)

To address these questions, we first empirically analyze the ADO problem. Our findings confirm the significance of ADO and further reveal two key insights: the effectiveness of distribution adjustments is indeed impacted by prompt updates, and a nested relationship exists between ADO and VPT. Based on these insights, we propose **PRO-VPT** (iterative Prompt Relocation-based VPT), a novel iterative framework derived from a nested optimization definition. Specifically, building on this definition, we develop a prompt relocation (**PR**) strategy for ADO, which comprises two optimization steps: pruning and allocating. The pruning step first identifies and releases idle prompts from prompt-saturated blocks, while the subsequent allocation step determines the most prompt-needed blocks for redistributing these prompts. By iteratively performing PR and VPT, PRO-VPT can adaptively learn the optimal prompt distribution for each task in a nested optimization manner, thereby unlocking the full potential of VPT. Our main contributions are fourfold.

- We explore the ADO problem within VPT and reveal the nested relationship between ADO and VPT.
- Building upon our insights into prompt distribution, we propose the first ADO-VPT co-design framework, termed PRO-VPT, with a nested optimization definition.
- Derived from the definition, we present a PR strategy for ADO, which introduces an idleness score to prune under-

utilized prompts from prompt-saturated blocks and then allocates them to prompt-needed blocks using reinforcement learning (RL).

- Extensive experiments show that PRO-VPT exhibits superior performance, *e.g.*, it attains state-of-the-art average accuracies of 78.0% on VTAB-1k and 91.7% on FGVC, with 1.6 pp and 2.0 pp advantages over the VPT baseline.

2. Related Work

Visual Prompt Tuning. VPT [22], one of the leading techniques in PEFT, draws inspiration from language-domain prompting works [19, 32, 37, 38] to fine-tune a small portion of prompts while keeping the pre-trained model frozen. Subsequent research has improved VPT in three main aspects: (1) Extending prompts to other Transformer components (*e.g.*, key and value matrices or the patch embedding layer) to better suit the Transformer architecture [13, 50, 52]; (2) Initializing prompts with prototypes of image tokens to accelerate convergence [58]; (3) Refining the propagation structures of prompts to strengthen cross-layer interactions [5, 63, 71]. However, most existing methods depend on a fixed prompt distribution for all tasks, resulting in less effective prompting performance. In contrast, our approach adaptively adjusts the prompt distribution for each task, enabling prompt-based methods to achieve state-of-the-art performance.

Layer-wise Fine-Tuning. Recent research has highlighted the importance of treating each pre-trained block differently during downstream fine-tuning, emphasizing the need for layer-wise adaptive strategies to calibrate the fine-tuning intensity for each block [12, 25, 31, 43, 54]. For instance, [29] first revealed that some pre-trained blocks may already be near-optimal for specific tasks, indicating that fine-tuning demands of each block vary significantly for different tasks. This work then proposes freezing these near-optimal blocks and selectively fine-tuning the remaining ones to improve performance. Similarly, [45, 49] proposes to adaptively assign different learning rates to each block, tailoring the fine-tuning intensity at a layer level to achieve more fine-grained layer-wise adaptation. Inspired by these findings, we hypothesize that the prompting intensity for each block, *i.e.*, the overall distribution of prompts, may also play a crucial role in task adaptation, leading us to focus on adaptively adjusting the prompt distribution within VPT.

3. Methodology

3.1. Notation

Visual prompt tuning (VPT) aims to learn lightweight tunable prompts \mathbf{P} that are inserted into the vision Transformer (ViT) $f(\cdot)$ with a specific distribution \mathcal{D} . In particular, for a set of N prompts $\mathbf{P} = \{\mathbf{p}_k\}_{k=1}^N$ and their distributed blocks $\mathcal{D} = \{d_k\}_{k=1}^N$ where $d_k \in \{0, 1, \dots, L\}$ ($d_k = 0$ for undistributed), the prompted ViT model is denoted as $f_{\mathbf{P}, \mathcal{D}}(\cdot)$. Given a training set \mathcal{T}_{tr} of input-label pairs (\mathbf{x}, y) , the model is then trained by minimizing the task loss $\mathcal{L}(f_{\mathbf{P}, \mathcal{D}}(\mathbf{x}), y)$.

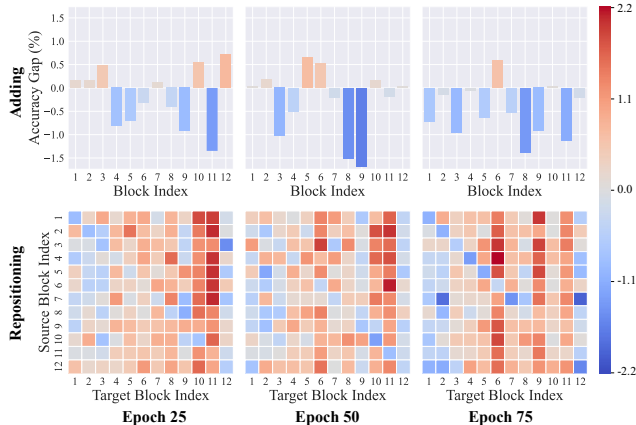


Figure 2. **Performance gaps from distribution adjustments using prompts from epochs 25, 50, and 75.** Adjusting prompt distribution appropriately leads to enhanced performance; however, effective adjustments vary significantly across different epochs.

For convenience in later sections, we define the loss difference as $\Delta\mathcal{L}(f_1, f_2) = \mathcal{L}(f_1(\mathbf{x}), y) - \mathcal{L}(f_2(\mathbf{x}), y)$.

3.2. Analysis and Formulation of ADO

We first explore the underlying nature of ADO and its formal definition, in response to question ①.

Intuitively, ADO can be defined in two distinct ways: **one-shot** (independently adjusting the distribution) or **iterative** (integrating with prompt tuning through iteratively adjusting the distribution). These definitions are distinct in whether the distribution is adjusted concurrently with prompt tuning. Specifically, an iterative process is more appropriate when distribution adjustments are affected by ongoing changes in prompts, as independent optimization may lead to sub-optimal results by failing to account for these dynamics. Otherwise, one-shot adjustments may be sufficient.

To investigate which definition better matches the underlying nature, we experiment to examine how distribution adjustments behave when applied to prompts from different epochs. We use two intuitive adjustment strategies: incrementally *adding* to a small initial prompt set and *repositioning* existing prompts. As shown in Fig. 2, adding or repositioning prompts to specific blocks can effectively improve performance; however, the effective adjustments differ significantly when prompts are updated. Comprehensive results with detailed analysis are provided in Appendix C. In conclusion, we summarize our key findings as follows:

Finding 1. *Properly adjusting the prompt distribution significantly enhances performance, confirming the necessity to reconsider its optimization.*

Finding 2. *Distribution adjustments are sensitive not only to different blocks but also to the updated prompts themselves, highlighting the need for an iterative process that continuously adjusts the distribution during training.*

Finding 3. *The effectiveness of distribution adjustments can only be properly evaluated after prompt tuning, indicating*

that the prompt tuning process should be nested within the distribution optimization process (see Appendix C).

Building on these insights, we propose integrating ADO with VPT into an **iterative** optimization framework. Formally, we present the definition of this ADO-VPT co-design framework through the lens of **nested** optimization, where the objectives of ADO and VPT are expressed as:

$$\mathcal{D}^* = \arg \min_{\mathcal{D}} \mathbb{E}_{(\mathbf{x}, y) \in \mathcal{T}_{tr}} [\mathcal{L}(f_{\mathbf{P}^*, \mathcal{D}}(\mathbf{x}), y)], \quad (1)$$

$$\mathbf{P}^* = \arg \min_{\mathbf{P}} \mathbb{E}_{(\mathbf{x}, y) \in \mathcal{T}_{tr}} [\mathcal{L}(f_{\mathbf{P}, \mathcal{D}^*}(\mathbf{x}), y)]. \quad (2)$$

This formulation clearly illustrates the intertwined relationship between visual prompts \mathbf{P} and their distribution \mathcal{D} , with its framework presented in Fig. iii. In this framework, prompt tuning is integrated into the ADO process, forming a closed-loop workflow of ‘distribution adjustment \rightarrow prompt tuning \rightarrow adjustment evaluation \rightarrow new adjustment’, thereby achieving a co-design process aligning with the observed iterative and nested nature.

Remark. This nested optimization framework offers a universal approach capable of incorporating various distribution adjustment strategies, *e.g.*, adding or repositioning. However, we empirically observe that adding-based adjustments often lead to unstable performance (see Appendix D). Therefore, in the following section, we focus on developing a prompt relocation (PR) strategy based on this formulation to effectively tackle the ADO problem.

3.3. Iterative Prompt Relocation-based VPT

Following the relocation objective defined in Eq. (1), we introduce the PR strategy derived from this definition and provide a detailed overview of the PRO-VPT framework, in response to question ②.

Building on the aforementioned findings, the *discrete* PR objective is further complicated by the *non-stationary* nature of effective relocation (**Finding 2**) and the necessity to *predict* the effectiveness of relocation operations (**Finding 3**). Nonetheless, these three properties make a RL framework [24, 33] a natural and well-suited approach for optimizing the PR objective. However, a naive RL implementation needs to model all possible relocation operations as actions, resulting in L^2 possible arrangements (*e.g.*, 144 actions for ViT-B). Such a large action space necessitates numerous iterations to achieve convergence (*cf.* § 4.3).

To address this, we propose decomposing the PR process into two sequential steps: **pruning** and **allocating**. The pruning step first identifies and releases idle prompts for relocation, while the allocating step then employs RL to determine optimal blocks for these freed prompts. By focusing solely on allocatable blocks instead of all block arrangements, this approach effectively reduces the action space from L^2 to L . More importantly, this approach has an intuitive explanation: idle prompts typically exist within the prompt-saturated

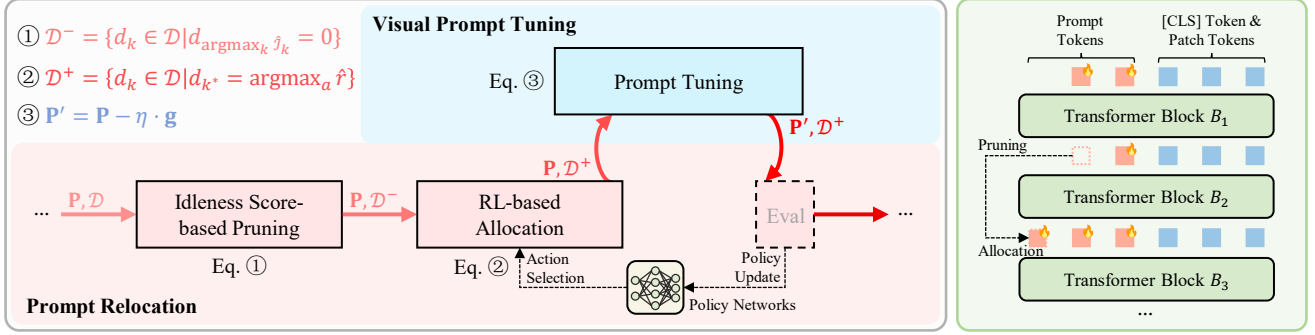


Figure 3. **Overview of our proposed PRO-VPT.** *Left:* The streamlined workflow of PRO-VPT. *Right:* Illustration of the PR process.

blocks, thus relocating them to prompt-needed blocks may enhance the effectiveness of prompt distribution. Decomposed from the relocation objective in Eq. (1), the pruning and allocation steps¹ can be formalized as:

$$k^* = \arg \max_k \mathbb{E}_{(\mathbf{x}, y) \in \mathcal{T}_{tr}} [\Delta \mathcal{L}(f_{\mathbf{P}, \mathcal{D}}, f_{\mathbf{P}, \mathcal{D} | d_k = 0})], \quad (3)$$

$$a^* = \arg \max_a \mathbb{E}_{(\mathbf{x}, y) \in \mathcal{T}_{tr}} [\Delta \mathcal{L}(f_{\mathbf{P}, \mathcal{D}^-}, f_{\mathbf{P}', \mathcal{D} | d_{k^*} = a})], \quad (4)$$

where $\mathcal{D}^- = \{d_k \in \mathcal{D} | d_{k^*} = 0\}$ and $\mathcal{D}^+ = \{d_k \in \mathcal{D} | d_{k^*} = a^*\}$ denote the prompt distributions after pruning and allocation with $a \in [L]$ as the allocation block, and the allocation step uses the tuned prompts \mathbf{P}' for evaluation following Finding 3. These two equations are specifically designed to identify the k^* -th prompt suitable for pruning and to determine the optimal block a^* for allocating.

Following this, we utilize Eqs. (3) and (4) to approach the pruning and allocation stages, respectively, with the overall PRO-VPT framework illustrated in Fig. 3 and Algo. i:

Idleness Score-based Pruning. To measure whether a prompt is idle for its current block and suitable for relocation, we take Eq. (3) as the idleness score:

$$\mathcal{I}_k = \Delta \mathcal{L}(f_{\mathbf{P}, \mathcal{D}}, f_{\mathbf{P}, \mathcal{D} | d_k = 0}). \quad (5)$$

Intuitive Interpretation. If $\mathcal{I}_k = \Delta \mathcal{L} > 0$, pruning the prompt \mathbf{p}_k from its current block can enhance performance. This indicates that \mathbf{p}_k is negative for its current block, which tends to be prompt-saturated and therefore suitable for its relocation to a more prompt-needed block. Conversely, $\mathcal{I}_k \leq 0 \forall k$ suggests that no blocks are saturated and thus the prompt distribution is near-optimal.

Pruning Implementation. Since computing \mathcal{I}_k for each individual prompt \mathbf{p}_k is significantly inefficient, we approximate \mathcal{I}_k using its first-order Taylor expansion (see Appendix F for detailed derivation):

$$\hat{\mathcal{I}}_k \approx \mathbf{g}_k^T \mathbf{p}_k, \quad (6)$$

where $\mathbf{g}_k = \frac{\nabla \mathcal{L}}{\nabla \mathbf{p}_k}$ represents the elements of the gradient \mathbf{g} .

¹Here, for simplicity and efficiency, both the pruning and allocation steps are formalized to operate on a single prompt per iteration, as further elaborated in Appendix E.

To this end, by calculating the estimated scores as in Eq. (6), we can effectively identify and prune the idle prompt \mathbf{p}_{k^*} with the maximum $\hat{\mathcal{I}}_{k^*}$ from the prompt-saturated block (when $\max \hat{\mathcal{I}}_k > 0$), thereby fulfilling Eq. (3) and forming the pruned distribution \mathcal{D}^- .

RL-based Allocation. After pruning an idle prompt, the following key step is to leverage RL to determine its optimal allocation to the prompt-needed block. Specifically, we take Eq. (4) as the optimization objective for the RL problem, *i.e.*, the allocation reward, as follows:

$$r = \Delta \mathcal{L}(f_{\mathbf{P}, \mathcal{D}^-}, f_{\mathbf{P}', \mathcal{D} | d_{k^*} = a}). \quad (7)$$

Intuitive Interpretation. The optimal allocation block a^* , which achieves the maximum $r^* = \max \Delta \mathcal{L}$, is identified as the block where assigning a prompt leads to the highest performance improvement, implying that this block is the most prompt-needed.

Allocation Implementation. We detail the RL-based allocation under a Markov decision process framework, where the main components are:

(1) **State.** We leverage all available information to represent the state of the current prompt distribution. Specifically, the state incorporates the block-wise idleness scores, the current distribution, and the pruned prompt's location, formally defined as $s = \{\sum_{d_k=i} \hat{\mathcal{I}}_k\}_{i=1}^L \cup \mathcal{D}^- \cup \text{OneHot}(k^*)$. After PR and VPT, the state transitions to s' .

(2) **Action.** The action determines which block the pruned prompt will be allocated to, represented as $a \in [L]$.

(3) **Reward.** Although the allocation reward r is defined in Eq. (7), calculating the intermediate loss of $f_{\mathbf{P}, \mathcal{D}^-}$ is computationally inefficient. To address this, we approximate r by incorporating the idleness score as:

$$\hat{r} \approx \Delta \mathcal{L}(f_{\mathbf{P}, \mathcal{D}}, f_{\mathbf{P}', \mathcal{D} | d_{k^*} = a}) - \hat{\mathcal{I}}_{k^*}, \quad (8)$$

where the idleness score $\hat{\mathcal{I}}_{k^*} \approx \Delta \mathcal{L}(f_{\mathbf{P}, \mathcal{D}}, f_{\mathbf{P}, \mathcal{D}^-})$ provides an approximation of the intermediate loss of $f_{\mathbf{P}, \mathcal{D}^-}$.

To this end, by leveraging RL to maximize the estimated reward as in Eq. (8), we can efficiently determine the optimal allocation to the prompt-needed block a^* even within the non-stationary environment, thereby fulfilling Eq. (4)

and forming the relocated distribution \mathcal{D}^+ . Particularly, we accomplish this by employing proximal policy optimization (PPO) [48], a state-of-the-art RL algorithm.

Remark. Although the relocation process is decomposed into two-step sequential steps, the overall optimization objective, whether based on the expected objectives in Eqs. (3) and (4) or the estimated objectives in Eqs. (6) and (8), can be expressed as $\max_{k,a} \mathbb{E}_{(\mathbf{x},y) \in \mathcal{T}_{tr}} [\Delta \mathcal{L}(f_{\mathcal{P},\mathcal{D}}, f_{\mathcal{P}',\mathcal{D}|d_k=a})]$. This formulation remains *equivalent* to the original PR objective (*i.e.*, the ADO objective) defined in Eq. (1). Consequently, leveraging the nested optimization formulation, the proposed PR strategy can effectively address the ADO problem and adaptively construct the optimal distribution.

3.4. Discussion

We note that some prior works have *indirectly* achieved adaptive distribution [13, 27, 67]. Specifically, pruning-based techniques [13, 27] introduce mask variables to iteratively prune redundant prompts from the original distribution, and NOAH [67] uses an evolutionary algorithm to search for an optimal sub-distribution within the original distribution in a one-shot manner. PRO-VPT is distinct and advantageous compared to these methods as:

Distinct Goals. These methods aim to enhance performance through the lottery ticket hypothesis [8, 41, 47], focusing on searching for a more effective sub-distribution within a given hyper-distribution by circumventing negative prompts and retaining essential ones. However, they are limited to pruning prompts from prompt-saturated blocks and fail to tackle prompt-deficient blocks (*cf.* § 4.5). In contrast, our approach actively learns an optimal distribution of all prompts, adaptively relocating them from prompt-saturated blocks to prompt-needed blocks through our PR strategy, thereby maximizing the effectiveness of the entire prompt distribution. This fundamental distinction sets our approach apart from the methods discussed above.

Efficient. While effective, we argue that these approaches typically incur considerable unnecessary training costs to identify an optimal sub-distribution, as numerous trained prompts are pruned and left unused (*cf.* § 4.3). This fundamentally contradicts the goal of parameter efficiency. Conversely, our work directly adjusts the distribution of the entire prompt set through prompt relocation, thereby minimizing extra costs and improving efficiency.

Effective. These methods straightforwardly apply one-shot or iterative processes without considering the underlying distribution dynamics. For instance, NOAH [67] adopts a one-shot approach post-training, leading to suboptimal results (*cf.* § 4.2). Conversely, our work conducts empirical analyses and accordingly proposes a *nested optimization-based* method, enabling prompt-based methods to reach state-of-the-art performance.

4. Experiments

4.1. Experiment Setups

Datasets. We evaluated our proposed PRO-VPT on a series of datasets grouped into three categories: (1) **VTAB-1k.** The visual task adaptation benchmark (VTAB) [66] encompasses 19 classification tasks categorized into three groups: *Natural*, *Specialized*, and *Structured*, aiming to assess adaptation capabilities under low-shot training conditions. (2) **FGVC.** Fine-grained visual classification (FGVC) includes 5 classification tasks: CUB-200-2011 [56], NABirds [55], Oxford Flowers [42], Stanford Dogs [6], and Stanford Cars [10], aiming to assess task adaptation in large-scale, fine-grained settings. (3) **COCO and ADE20k.** These widely-used benchmarks for detection and segmentation are employed to assess the generalizability of our method across diverse downstream visual tasks.

Implementation Details. We mainly use ViT-B/16 [7] supervised pre-trained on ImageNet-21k [46] as the initialization. We employ the SGD optimizer with a batch size of 64 and fine-tune models for 100 epochs. The number of prompt tokens per task in our method is set in accordance with [22]. Following [51], we evaluate our method using Inception normalization instead of ImageNet normalization, and for fair comparisons, we present the results of other counterparts using both normalization techniques. Notably, unlike most approaches [9, 22, 34, 68], our method employs a fixed learning rate instead of using a learning rate schedule, as we necessitate ensuring timely rewinding after prompt relocation [44]. More details about the hyper-parameters are provided in Appendices G.

4.2. Main Results

VTAB-1k. We evaluate the proposed PRO-VPT on VTAB-1k and compare it with other methods. We provide results for *full* fine-tuning and *linear* probing as baselines of traditional fine-tuning. As competing advanced adapter- or reparameterization-based methods, we include SSF [34], SPT-Adapter [16], Adapter+ [51], LoRA [20], FacT-TK [23], and Consolidator [15]. Furthermore, we benchmark against state-of-the-art prompt-based methods including VPT [22], NOAH [67], SPT [58], and iVPT [71].

Tab. 1 presents results on VTAB-1k with the best-performing normalization techniques (*i.e.*, ImageNet or Inception) for each method (see Appendix H for complete results). Among all prompt-based methods, the previous best performance of 77.1% average accuracy achieved by iVPT falls short of the advanced adapter-based method Adapter+, which reaches 77.6%. Nevertheless, with the introduction of the optimization-based adaptive distribution, the proposed PRO-VPT sets a new state-of-the-art performance among all evaluated methods with an average accuracy of 78.0%, highlighting the significant potential of prompt-based approaches. Additionally, compared to the one-shot optimization-based

Table 1. **Detailed results on the VTAB-1k datasets.** Performance results are reported as the highest of ImageNet normalization (◦) or Inception normalization (●), presented in % after a complete training schedule with ViT-B/16 supervised pre-trained on ImageNet-21k. The best results of prompt-based methods and other PEFT approaches are highlighted in **bold**. ‡: Early-stopping based on the test set. †: Lack of complete code or hyperparameter configurations for the method, hence results are reported as presented in the original paper. ¹Average across the average accuracies of the VTAB-1k groups, following previous work.

	Param (M)	Natural							Specialized				Structured							Global Avg. ¹				
		Cifar100	Caltech101	DTD	Flower102	Pets	SVHN	Sun397	Group Avg.	Camelyon	EuroSAT	Resisc45	Retinopathy	Group Avg.	Clevr-Count	Clevr-Dist.	DMLab	KITTT-Dist.	dSpr-Loc.		dSpr-Ori.	sNORB-Azi.	sNORB-Ele.	Group Avg.
Full ●	85.8	73.2	92.6	70.4	97.9	86.2	90.6	39.6	78.6	87.1	96.6	87.5	74.0	86.3	66.6	61.0	49.8	79.7	82.6	51.9	33.5	37.0	57.8	74.2
Linear ●	0.04	78.1	88.1	69.0	99.1	90.0	36.0	56.9	73.9	79.8	90.7	73.7	73.7	79.5	32.4	30.5	35.9	61.9	11.2	26.2	14.3	24.5	29.6	61.0
LoRA ● [20]	0.29	83.0	91.7	71.6	99.2	90.9	83.8	56.7	82.4	86.2	95.7	83.5	71.9	84.3	77.7	62.3	49.0	80.2	82.2	51.7	31.0	47.0	60.1	75.6
FacT-TK ₈ ● [23]	0.05	74.9	92.7	73.7	99.1	91.3	85.5	57.7	82.1	86.8	94.9	84.1	70.9	84.2	81.9	64.1	49.2	77.2	83.8	53.1	28.2	44.7	60.3	75.5
FacT-TK _{≤32} ● [23]	0.10	74.6	93.7	73.6	99.3	90.6	88.7	57.5	82.6	87.6	95.4	85.5	70.4	84.7	84.3	62.6	51.9	79.2	85.5	52.0	36.4	46.6	62.3	76.5
Consolidator † [15]	0.30	74.2	90.9	73.9	99.4	91.6	91.5	55.5	82.4	86.9	95.7	86.6	75.9	86.3	81.2	68.2	51.6	83.5	79.8	52.3	31.9	38.5	60.9	76.5
SSF † [34]	0.24	69.0	92.6	75.1	99.4	91.8	90.2	52.9	81.6	87.4	95.9	87.4	75.5	86.6	75.9	62.3	53.3	80.6	77.3	54.9	29.5	37.9	59.0	75.7
SPT-Adapter † [16]	0.23	72.9	93.2	72.5	99.3	91.4	84.6	55.2	81.3	85.3	96.0	84.3	75.5	85.3	82.2	68.0	49.3	80.0	82.4	51.9	31.7	41.2	60.8	75.8
SPT-Adapter † [16]	0.43	72.9	93.2	72.5	99.3	91.4	88.8	55.8	82.0	86.2	96.1	85.5	75.5	85.8	83.0	68.0	51.9	81.2	82.4	51.9	31.7	41.2	61.4	76.4
Adapter+ _{r=16} ● [51]	0.35	83.7	94.2	71.5	99.3	90.6	88.2	55.8	83.3	87.5	97.0	87.4	72.9	86.2	82.9	60.9	53.7	80.8	88.4	55.2	37.3	46.9	63.3	77.6
Prompt-based Methods:																								
VPT-Deep ● [22]	0.60	83.0	93.0	71.2	99.0	91.3	84.1	56.0	82.5	84.9	96.6	82.5	74.5	84.6	77.5	58.7	49.7	79.6	86.2	56.1	37.9	50.7	62.1	76.4
NOAH † [67]	0.43	69.6	92.7	70.2	99.1	90.4	86.1	53.7	80.2	84.4	95.4	83.9	75.8	84.9	82.8	68.9	49.9	81.7	81.8	48.3	32.8	44.2	61.3	75.5
SPT-Deep † [58]	0.22	79.3	92.6	73.2	99.5	91.0	89.1	51.2	82.3	85.4	96.8	84.9	74.8	85.5	70.3	64.8	54.2	75.2	79.3	49.5	36.5	41.5	58.9	75.6
iVPT † [71]	0.60	82.7	94.2	72.0	99.1	91.8	88.1	56.6	83.5	87.7	96.1	87.1	77.6	87.1	77.1	62.6	49.4	80.6	82.1	55.3	31.8	47.6	60.8	77.1
PRO-VPT (ours)	0.61	84.5	94.1	73.2	99.4	91.8	88.2	57.2	84.1	87.7	96.8	86.6	75.5	86.7	78.8	61.0	50.6	81.3	86.7	56.4	38.1	51.7	63.1	78.0

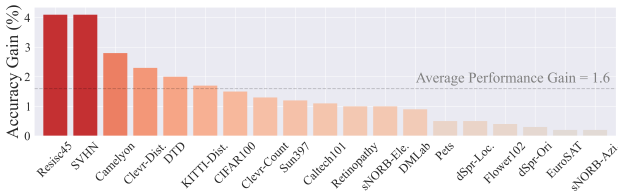


Figure 4. **Performance gains** achieved by VPT w/ ADO (PRO-VPT) compared to VPT w/o ADO (VPT-Deep). PRO-VPT consistently outperforms VPT-Deep.

NOAH, our nested optimization-based PRO-VPT achieves an average accuracy gain of 2.5 pp, validating the effectiveness of our proposed nested optimization framework.

Furthermore, Fig. 4 illustrates the performance differences between VPT w/ ADO (PRO-VPT) and w/o ADO (VPT-Deep) on the VTAB-1k datasets. The accuracies of PRO-VPT are consistently higher than those of VPT-Deep, yielding an average accuracy improvement of 1.6 pp. This emphasizes the significance of optimizing the prompt distribution to unlock the full potential of VPT.

FGVC. Next, we evaluate PRO-VPT on the FGVC benchmark. Among the aforementioned contenders, only a portion have conducted evaluations on FGVC and released the code and configurations.

Tab. 2 presents the FGVC results with the best-performing normalization (see Appendix H for complete results). PRO-VPT achieves the best average accuracy of 91.7% over all five FGVC datasets, surpassing the second-best performance of 91.4% achieved by Adapter+ and SPT-Deep. This demonstrates that PRO-VPT also delivers state-of-the-art results for task adaptation when training data is large-scale.

Table 2. **Detailed results on the FGVC datasets.** Performance results are reported as the highest of ImageNet normalization (◦) or Inception normalization (●), presented in % after a complete training schedule with ViT-B/16 supervised pre-trained on ImageNet-21k. The best results of prompt-based methods and other PEFT approaches are highlighted in **bold**. †: Same as Tab. 1.

	Param (M)	CUB200	NABirds	Oxford Flowers	Stanford Dogs	Stanford Cars	Global Avg.
Full ●	86.0	88.0	81.5	99.2	85.6	90.6	89.0
Linear ●	0.18	88.9	81.8	99.5	92.6	52.8	83.1
SSF ◦ [34]	0.39	89.5	85.7	99.6	89.6	89.2	90.7
SPT-Adapter † [16]	0.40	89.1	83.3	99.2	91.1	86.2	89.8
SPT-LoRA † [16]	0.52	88.6	83.4	99.5	91.4	87.3	90.1
Adapter+ ● [51]	0.34	90.4	85.0	99.7	92.6	89.1	91.4
Prompt-based Methods:							
VPT-Deep ● [22]	0.85	90.1	83.3	99.6	90.3	85.0	89.7
SPT-Deep † [58]	0.36	90.6	87.6	99.8	89.8	89.2	91.4
iVPT † [71]	0.41	89.1	84.5	99.5	90.8	85.6	89.9
PRO-VPT (ours)	0.86	90.6	86.7	99.7	91.8	89.6	91.7

4.3. Ablation Study

To comprehensively assess the advantages of our proposed PR strategy, we compare it with the following alternative strategies, as shown in Tab. 3:

Strategies (A), (B) represent alternatives for extracting a sub-distribution from a hyper-distribution (see § 3.4). We utilize the pruning-based technique as in [13], applying pruning percentages ranging from 10% to 90% with 10 pp intervals. (B) prunes from a huge hyper-distribution to obtain a sub-distribution with the same *final* parameter count as the VPT

Table 3. **Ablation study on various alternative ADO strategies.** Results are presented using ViT-B/16 on two instances: *Natural* SVHN and *Specialized* Resisc45. The best and second-best results are highlighted in **bold** and underline. *Our proposed PR strategy.

Alternatives for the ADO Problem	SVHN		Resisc45	
	Param (M)	Acc (%)	Param (M)	Acc (%)
VPT Baseline	0.468	84.10	0.127	82.50
(A) Pruning	0.468	83.76	0.127	83.81
(B) Pruning	2.543	84.17	0.541	84.86
(C) <i>Naive RL</i>	<u>0.482</u>	83.51	<u>0.140</u>	83.02
(D) <i>Prn1 & Alc1</i>	0.468	84.88	0.127	84.06
(E) <i>Prn1 & Alc2</i>	<u>0.482</u>	<u>86.99</u>	<u>0.140</u>	<u>85.68</u>
(F) <i>Prn2 & Alc1</i>	0.468	85.82	0.127	84.76
(G) <i>Prn2 & Alc2*</i>	<u>0.482</u>	88.19	<u>0.140</u>	86.56

baseline, and (A) prunes from a smaller hyper-distribution to match the number of *trained* parameters in the VPT baseline.

Strategies (C)-(G) represent alternatives of prompt relocating, each incorporating different components. Particularly, (C) frames the PR process as a *naive RL* problem (see § 3.3) and utilizes the PPO algorithm. (D)-(G) are various combinations of the following components:

Prn1. Randomly pruning prompts.

Prn2. Pruning underutilized prompts based on the idleness score.

Alc1. Modeling the allocation task as a multi-armed bandit problem, which is well-suited for stationary discrete decision-making, and then adopting the widely used Thompson sampling for prompt allocation.

Alc2. Modeling the allocation task as a vanilla RL problem, which is more suited to non-stationary decision-making, and then using the popular PPO algorithm for prompt allocation.

In summary, the key observations are as follows:

Observation 1. *Relocation-based methods are more efficient and effective compared to pruning-based methods.* Pruning strategies (A) and (B) typically underperform relocation strategies (D)-(G), indicating that pruning is less effective in adaptive distribution. Specific to pruning, while (B) outperforms (A), it incurs high storage costs (*e.g.*, 2.075M trained but unused parameters in SVHN) and still lags behind our proposed PR strategy. In contrast, RL-based relocation strategies (E) and (G) require only 0.014M extra parameters for PPO’s policy networks, which is relatively negligible.

Observation 2. *The decomposition for RL is remarkably effective.* Strategy (C) significantly underperforms the two-step PR strategies (D)-(G), underscoring the benefits of decomposing the PR process for simplifying decision-making.

Observation 3. *Both the pruning and allocation components in PRO-VPT exhibit significantly effective, especially RL-based allocation.* Comparing strategies (D) vs. (F) and (E) vs. (G), *Prn2* indicates superior performance improvements (averaging 1.07 pp for SVHN and 0.79 pp for Resisc45), highlighting the effectiveness of the proposed idleness score. Moreover, strategies (G) and (E) achieve the best results, with *Alc2* delivering remarkable gains over *Alc1* (2.24 pp and 1.71 pp), highlighting the advantage of framing the allocation task as a non-stationary RL problem.

Table 4. **Generalizability study on distinct backbones.** Results are presented in % on two instances: VTAB-1k *Natural* Cifar100 and *Structured* DMLab.

Backbone		Cifar100	DMLab
ViT-B/16	VPT-Deep	83.00	49.70
	PRO-VPT	84.49 1.49 ↑	50.64 0.94 ↑
ViT-L/16	VPT-Deep	85.82	45.98
	PRO-VPT	87.07 1.25 ↑	46.57 0.59 ↑
ViT-H/14	VPT-Deep	78.49	44.12
	PRO-VPT	79.73 1.24 ↑	45.17 1.05 ↑
Swin-B	VPT-Deep	81.33	49.86
	PRO-VPT	82.67 1.34 ↑	50.78 0.92 ↑

Table 5. **Generalizability study on different pre-training strategies.** Results are presented in % on two instances: VTAB-1k *Natural* Cifar100 and *Structured* DMLab.

Pre-Training Strategy		Cifar100	DMLab
Supervised	VPT-Deep	83.00	49.70
	PRO-VPT	84.49 1.49 ↑	50.64 0.94 ↑
Self-Supervised:			
MAE	VPT-Deep	32.65	43.58
	PRO-VPT	34.36 1.71 ↑	46.07 2.49 ↑
MoCo-v3	VPT-Deep	72.48	46.56
	PRO-VPT	73.62 1.14 ↑	47.63 1.07 ↑

4.4. Generalizability Analysis

We evaluate the generalizability of PRO-VPT across different backbones and pre-training strategies, as well as in detection and segmentation tasks.

Backbone. We experiment with three different scales of the ViT backbone: ViT-Base (ViT-B/16), ViT-Large (ViT-L/16), and ViT-Huge (ViT-H/14) [7], along with the hierarchical Swin Transformer (Swin-B) [39]. All backbones are supervised pre-trained on ImageNet-21k [46]. As shown in Tab. 4, PRO-VPT delivers higher accuracy compared to VPT with various scales and architectures.

Pre-Training Strategy. In addition to the supervised pre-training strategy, we experiment with two self-supervised strategies: the masked image modeling method (MAE) [18] and the contrastive self-supervised method (MoCo-v3) [3]. As illustrated in Tab. 5, PRO-VPT consistently outperforms VPT regardless of the pre-training strategy, highlighting its strong generalizability.

Detection and Segmentation. We also experiment on detection and segmentation tasks in Appendix H, where PRO-VPT still maintains advantages over VPT.

4.5. Observations on PRO-VPT

We design several experiments to thoroughly understand PRO-VPT. The key insights are concluded as follows:

Observation 1. *PRO-VPT effectively learns task-specific prompt distributions.* We visualize the learned distributions of PRO-VPT under different total numbers of prompts, as shown in Fig. 5. Notably, the distributions remain consistent

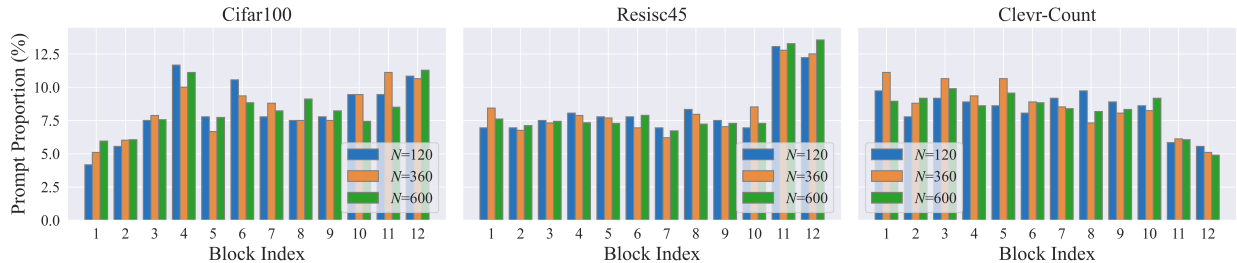


Figure 5. **Visualization of prompt distributions learned by PRO-VPT on VTAB-1k Natural** Cifar100, *Specialized* Resisc45, and *Structured* Clevr-Count with varying numbers of prompts. PRO-VPT effectively learns task-specific distributions.

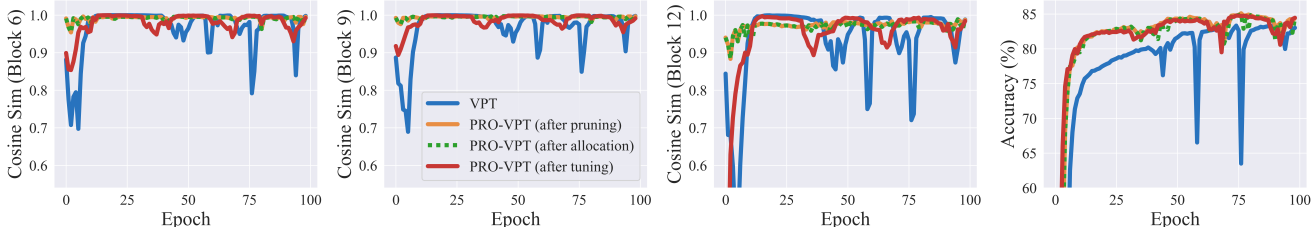


Figure 7. **Cosine similarity of feature changes and the corresponding test accuracy.** The PR strategy has a minimal impact on features, and PRO-VPT demonstrates better stability than VPT in both representation and performance.

across different prompt numbers but exhibit significant variations across different tasks. This indicates that the prompting importance of each block indeed varies by task, and PRO-VPT effectively captures and adapts to these task-specific distributions to better accommodate each task.

Observation 2. *PRO-VPT effectively meets the block-specific prompt requirements via prompt relocation.* We visualize the attention weights from representation features (*i.e.*, [CLS] embeddings) to prompts across different blocks on Cifar100. Each attention weight represents the importance of a given prompt for its corresponding block. As depicted in Fig. 6, the attention weights in VPT reveal phenomena of prompt saturation (*e.g.*, blocks 2 and 5) and prompt deficiency (*e.g.*, blocks 4 and 12), confirming that different blocks exhibit significantly varying prompt demands. However, due to its fixed prompt distribution, VPT lacks the flexibility to adapt to these diverse needs. Even pruning-based methods can only prune negative prompts from prompt-saturated blocks while failing to address prompt-deficient blocks. In contrast, PRO-VPT effectively meets these block-specific prompt demands through adaptive prompt relocation. Such a fine-grained tuning strategy maximizes the effectiveness of the prompt distribution, thereby enhancing downstream task performance.

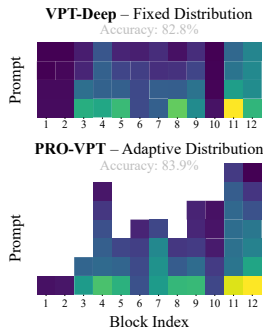


Figure 6. **Visualization of prompt attention weights.**

Observation 3. *PRO-VPT demonstrates enhanced stability and robustness.* One might be skeptical that runtime modifi-

cations of the prompt distribution could compromise stability. To investigate this, we evaluate both the representation stability and performance stability in PRO-VPT and VPT. Specific to feature stability, we measure cosine similarity between representations (*i.e.*, [CLS] embeddings) from the previous epoch and after each stage of pruning, allocation, and tuning. This similarity reflects the extent of feature changes resulting from each stage. Fig. 7 illustrates the similarity at different blocks and the corresponding test accuracy on Cifar100. Surprisingly, the orange and green lines indicate that the PR strategy has little impact on the learned features, as the features remain nearly unchanged after pruning and allocation. Moreover, PRO-VPT exhibits superior stability compared to VPT, both in terms of representation stability and performance stability. Additionally, as shown in Fig. vi, PRO-VPT demonstrates remarkable robustness to variations in prompt quantity compared to VPT, whereas the performance of VPT fluctuates significantly while PRO-VPT remains consistent. Overall, we argue that these benefits stem from our proposed *optimization-based* approach, which effectively identifies the optimal road for relocation, thereby minimizing its impact on stability and enhancing robustness.

5. Conclusion

This paper investigates the ADO problem within VPT. Based on our experimental insights into the nested relationship between ADO and VPT, we formalize an ADO-VPT co-design framework through the lens of nested optimization. Upon this formalization, we propose a novel PRO-VPT algorithm, which iteratively optimizes the distribution by integrating the PR (prompt relocation) strategy with VPT. Across 26 datasets, we show our method’s significant performance improvement over VPT with superior robustness.

Acknowledgements

This work was supported in part by the National Natural Science Foundation of China under Grants 62376233, 62306181, 62476063, and 62306313; in part by the NSFC / Research Grants Council (RGC) Joint Research Scheme under Grant N_HKBU214/21; in part by the General Research Fund of RGC under the Grant 12202622; in part by the RGC Senior Research Fellow Scheme under Grant SRFS2324-2S02; in part by the Guangdong Basic and Applied Basic Research Foundation under Grant 2024A1515010163; in part by the National Key Laboratory of Radar Signal Processing under Grant JKW202403; and in part by Xiaomi Young Talents Program.

References

- [1] Aochuan Chen, Yuguang Yao, Pin-Yu Chen, Yihua Zhang, and Sijia Liu. Understanding and improving visual prompting: A label-mapping perspective. In *CVPR*, pages 19133–19143, 2023. [1](#)
- [2] Shoufa Chen, Chongjian Ge, Zhan Tong, Jiangliu Wang, Yibing Song, Jue Wang, and Ping Luo. Adaptformer: Adapting vision transformers for scalable visual recognition. In *NeurIPS*, pages 16664–16678, 2022. [1](#)
- [3] Xinlei Chen, Saining Xie, and Kaiming He. An empirical study of training self-supervised vision transformers. In *CVPR*, pages 9640–9649, 2021. [7](#)
- [4] Timothée Darcet, Maxime Oquab, Julien Mairal, and Piotr Bojanowski. Vision transformers need registers. In *ICLR*, 2024. [vii](#)
- [5] Rajshekhar Das, Yonatan Dukler, Avinash Ravichandran, and Ashwin Swaminathan. Learning expressive prompting with residuals for vision transformers. In *CVPR*, pages 3366–3377, 2023. [2](#)
- [6] E Dataset. Novel datasets for fine-grained image categorization. In *CVPR Workshop on Fine-grained Visual Classification*, 2011. [5, v](#)
- [7] Alexey Dosovitskiy, Lucas Beyer, Alexander Kolesnikov, Dirk Weissenborn, Xiaohua Zhai, Thomas Unterthiner, Mostafa Dehghani, Matthias Minderer, Georg Heigold, Sylvain Gelly, et al. An image is worth 16x16 words: Transformers for image recognition at scale. In *ICLR*, 2020. [5, 7, i](#)
- [8] Jonathan Frankle and Michael Carbin. The lottery ticket hypothesis: Finding sparse, trainable neural networks. In *ICLR*, 2019. [5](#)
- [9] Minghao Fu, Ke Zhu, and Jianxin Wu. Dtl: Disentangled transfer learning for visual recognition. In *AAAI*, pages 12082–12090, 2024. [5](#)
- [10] Timnit Gebru, Jonathan Krause, Yilun Wang, Duyun Chen, Jia Deng, and Li Fei-Fei. Fine-grained car detection for visual census estimation. In *AAAI*, 2017. [5, v](#)
- [11] Henry Gouk, Timothy Hospedales, and massimiliano pontil. Distance-based regularisation of deep networks for finetuning. In *ICLR*, 2021. [2](#)
- [12] Yunhui Guo, Honghui Shi, Abhishek Kumar, Kristen Grauman, Tajana Rosing, and Rogerio Feris. Spottune: transfer learning through adaptive fine-tuning. In *CVPR*, pages 4805–4814, 2019. [2](#)
- [13] Cheng Han, Qifan Wang, Yiming Cui, Zhiwen Cao, Wenguan Wang, Siyuan Qi, and Dongfang Liu. E²vpt: An effective and efficient approach for visual prompt tuning. In *ICCV*, pages 17445–17456, 2023. [2, 5, 6, iv](#)
- [14] Cheng Han, Qifan Wang, Yiming Cui, Wenguan Wang, Lifu Huang, Siyuan Qi, and Dongfang Liu. Facing the elephant in the room: Visual prompt tuning or full finetuning? In *ICLR*, 2024. [1](#)
- [15] Tianxiang Hao, Hui Chen, Yuchen Guo, and Guiguang Ding. Consolidator: Mergable adapter with group connections for visual adaptation. In *ICLR*, 2023. [5, 6, vi](#)
- [16] Haoyu He, Jianfei Cai, Jing Zhang, Dacheng Tao, and Bohan Zhuang. Sensitivity-aware visual parameter-efficient finetuning. In *ICCV*, pages 11825–11835, 2023. [5, 6, vi, vii](#)
- [17] Kaiming He, Georgia Gkioxari, Piotr Dollár, and Ross Girshick. Mask r-cnn. In *ICCV*, pages 2961–2969, 2017. [v](#)
- [18] Kaiming He, Xinlei Chen, Saining Xie, Yanghao Li, Piotr Dollár, and Ross Girshick. Masked autoencoders are scalable vision learners. In *CVPR*, pages 16000–16009, 2022. [7](#)
- [19] Shihao Hou, Xinyi Shang, Shreyank N Gowda, Yang Lu, Chao Wu, Yan Yan, and Hanzi Wang. Capt: Class-aware prompt tuning for federated long-tailed learning with vision-language model. *arXiv preprint arXiv:2503.06993*, 2025. [2](#)
- [20] Edward J Hu, yelong shen, Phillip Wallis, Zeyuan Allen-Zhu, Yuanzhi Li, Shean Wang, Lu Wang, and Weizhu Chen. LoRA: Low-rank adaptation of large language models. In *ICLR*, 2022. [1, 5, 6, vi](#)
- [21] Lingyun Huang, Jianxu Mao, Yaonan Wang, Junfei Yi, and Ziming Tao. Cvpt: Cross-attention help visual prompt tuning adapt visual task. *arXiv preprint arXiv:2408.14961*, 2024. [vi, vii](#)
- [22] Menglin Jia, Luming Tang, Bor-Chun Chen, Claire Cardie, Serge Belongie, Bharath Hariharan, and Ser-Nam Lim. Visual prompt tuning. In *ECCV*, pages 709–727, 2022. [1, 2, 5, 6, i, iv, v, vi, vii, viii](#)
- [23] Shibo Jie and Zhi-Hong Deng. Fact: Factor-tuning for lightweight adaptation on vision transformer. In *AAAI*, pages 1060–1068, 2023. [5, 6, vi](#)
- [24] Leslie Pack Kaelbling, Michael L Littman, and Andrew W Moore. Reinforcement learning: A survey. *Journal of Artificial Intelligence Research*, 4:237–285, 1996. [3](#)
- [25] Gal Kaplun, Andrey Gurevich, Tal Swisa, Mazor David, Shai Shalev-Shwartz, and Eran Malach. Less is more: Selective layer finetuning with subtuning. *arXiv preprint arXiv:2302.06354*, 2023. [2](#)
- [26] Salman Khan, Muzammal Naseer, Munawar Hayat, Syed Waqas Zamir, Fahad Shahbaz Khan, and Mubarak Shah. Transformers in vision: A survey. *CSUR*, 54(10s):1–41, 2022. [1, i](#)
- [27] Youngeun Kim, Yuhang Li, Abhishek Moitra, Ruokai Yin, and Priyadarshini Panda. Do we really need a large number of visual prompts? *Neural Networks*, 177:106390, 2024. [5](#)

- [28] Yunyong Ko, Dongwon Lee, and Sang-Wook Kim. Not all layers are equal: A layer-wise adaptive approach toward large-scale dnn training. In *WWW*, pages 1851–1859, 2022. [2](#)
- [29] Yoonho Lee, Annie S Chen, Fahim Tajwar, Ananya Kumar, Huaxiu Yao, Percy Liang, and Chelsea Finn. Surgical fine-tuning improves adaptation to distribution shifts. In *ICLR*, 2023. [2](#)
- [30] Mengke Li, Ye Liu, Yang Lu, Yiqun Zhang, Yiu-ming Cheng, and Hui Huang. Improving visual prompt tuning by gaussian neighborhood minimization for long-tailed visual recognition. In *NeurIPS*, pages 103985–104009, 2024. [1](#)
- [31] Xingjian Li, Haoyi Xiong, Hanchao Wang, Yuxuan Rao, Liping Liu, Zeyu Chen, and Jun Huan. Delta: Deep learning transfer using feature map with attention for convolutional networks. In *ICLR*, 2019. [2](#)
- [32] Xiang Lisa Li and Percy Liang. Prefix-tuning: Optimizing continuous prompts for generation. In *ACL*, pages 4582–4597, 2021. [2](#)
- [33] Yuxi Li. Deep reinforcement learning: An overview. *arXiv preprint arXiv:1701.07274*, 2017. [3](#)
- [34] Dongze Lian, Daquan Zhou, Jiashi Feng, and Xinchao Wang. Scaling & shifting your features: A new baseline for efficient model tuning. In *NeurIPS*, pages 109–123, 2022. [5](#), [6](#), [vi](#), [vii](#)
- [35] Siyu Lin and Peter A Beling. An end-to-end optimal trade execution framework based on proximal policy optimization. In *IJCAI*, pages 4548–4554, 2021. [i](#)
- [36] Tsung-Yi Lin, Michael Maire, Serge Belongie, James Hays, Pietro Perona, Deva Ramanan, Piotr Dollár, and C Lawrence Zitnick. Microsoft coco: Common objects in context. In *ECCV*, pages 740–755. Springer, 2014. [v](#)
- [37] Pengfei Liu, Weizhe Yuan, Jinlan Fu, Zhengbao Jiang, Hiroaki Hayashi, and Graham Neubig. Pre-train, prompt, and predict: A systematic survey of prompting methods in natural language processing. *CSUR*, 55(9):1–35, 2023. [2](#)
- [38] Xiao Liu, Kaixuan Ji, Yicheng Fu, Weng Tam, Zhengxiao Du, Zhilin Yang, and Jie Tang. P-tuning: Prompt tuning can be comparable to fine-tuning across scales and tasks. In *ACL*, pages 61–68, 2022. [2](#)
- [39] Ze Liu, Yutong Lin, Yue Cao, Han Hu, Yixuan Wei, Zheng Zhang, Stephen Lin, and Baining Guo. Swin transformer: Hierarchical vision transformer using shifted windows. In *ICCV*, pages 10012–10022, 2021. [7](#)
- [40] Fang Ma, Chen Zhang, Lei Ren, Jingang Wang, Qifan Wang, Wei Wu, Xiaojun Quan, and Dawei Song. XPrompt: Exploring the extreme of prompt tuning. In *EMNLP*, pages 11033–11047, 2022. [1](#)
- [41] Eran Malach, Gilad Yehudai, Shai Shalev-Schwartz, and Ohad Shamir. Proving the lottery ticket hypothesis: Pruning is all you need. In *ICML*, pages 6682–6691, 2020. [5](#)
- [42] Maria-Elena Nilsback and Andrew Zisserman. Automated flower classification over a large number of classes. In *ICVGIP*, pages 722–729, 2008. [5](#), [v](#)
- [43] Junyoung Park, Jin Kim, Hyeongjun Kwon, Ilhoon Yoon, and Kwanghoon Sohn. Layer-wise auto-weighting for non-stationary test-time adaptation. In *WACV*, pages 1414–1423, 2024. [2](#)
- [44] Alex Renda, Jonathan Frankle, and Michael Carbin. Comparing rewinding and fine-tuning in neural network pruning. *arXiv preprint arXiv:2003.02389*, 2020. [5](#)
- [45] Youngmin Ro and Jin Young Choi. Autolr: Layer-wise pruning and auto-tuning of learning rates in fine-tuning of deep networks. In *AAAI*, pages 2486–2494, 2021. [2](#)
- [46] Olga Russakovsky, Jia Deng, Hao Su, Jonathan Krause, Sanjeev Satheesh, Sean Ma, Zhiheng Huang, Andrej Karpathy, Aditya Khosla, Michael Bernstein, et al. Imagenet large scale visual recognition challenge. *IJCV*, 115:211–252, 2015. [5](#), [7](#)
- [47] Pedro Savarese, Hugo Silva, and Michael Maire. Winning the lottery with continuous sparsification. In *NeurIPS*, pages 11380–11390, 2020. [5](#)
- [48] John Schulman, Filip Wolski, Prafulla Dhariwal, Alec Radford, and Oleg Klimov. Proximal policy optimization algorithms. *arXiv preprint arXiv:1707.06347*, 2017. [5](#), [i](#)
- [49] Zhiqiang Shen, Zechun Liu, Jie Qin, Marios Savvides, and Kwang-Ting Cheng. Partial is better than all: Revisiting fine-tuning strategy for few-shot learning. In *AAAI*, pages 9594–9602, 2021. [2](#)
- [50] Zhengxiang Shi and Aldo Lipani. Dept: Decomposed prompt tuning for parameter-efficient fine-tuning. In *ICLR*, 2024. [2](#)
- [51] Jan-Martin O Steitz and Stefan Roth. Adapters strike back. In *CVPR*, pages 23449–23459, 2024. [5](#), [6](#), [iv](#), [v](#), [vi](#), [vii](#)
- [52] Pengwei Tang, Xiaolin Hu, and Yong Liu. Adept: Adaptive decomposed prompt tuning for parameter-efficient fine-tuning. *arXiv preprint arXiv:2501.03291*, 2025. [2](#)
- [53] Junjiao Tian, Zecheng He, Xiaoliang Dai, Chih-Yao Ma, Yen-Cheng Liu, and Zsolt Kira. Trainable projected gradient method for robust fine-tuning. In *CVPR*, pages 7836–7845, 2023. [2](#)
- [54] Junjiao Tian, Yen-Cheng Liu, James S Smith, and Zsolt Kira. Fast trainable projection for robust fine-tuning. In *NeurIPS*, 2024. [2](#)
- [55] Grant Van Horn, Steve Branson, Ryan Farrell, Scott Haber, Jessie Barry, Panos Ipeirotis, Pietro Perona, and Serge Belongie. Building a bird recognition app and large scale dataset with citizen scientists: The fine print in fine-grained dataset collection. In *CVPR*, pages 595–604, 2015. [5](#), [v](#)
- [56] Catherine Wah, Steve Branson, Peter Welinder, Pietro Perona, and Serge Belongie. The caltech-ucsd birds-200-2011 dataset. *Technical report*, 2011. [5](#), [v](#)
- [57] Shaowen Wang, Linxi Yu, and Jian Li. Lora-ga: Low-rank adaptation with gradient approximation. In *NeurIPS*, pages 54905–54931, 2025. [1](#)
- [58] Yuzhu Wang, Lechao Cheng, Chaowei Fang, Dingwen Zhang, Manni Duan, and Meng Wang. Revisiting the power of prompt for visual tuning. In *ICML*, pages 50233–50247, 2024. [2](#), [5](#), [6](#), [vi](#), [vii](#)
- [59] Yuzhu Wang, Manni Duan, and Shu Kong. Attention to burstiness: Low-rank bilinear prompt tuning. *arXiv preprint arXiv:2506.22908*, 2025. [iv](#)
- [60] Raphael Ngigi Wanjiku, Lawrence Nderu, and Michael Kimwele. Dynamic fine-tuning layer selection using kullback-leibler divergence. *Engineering Reports*, 5(5):e12595, 2023. [2](#)

- [61] Yi Xin, Siqi Luo, Haodi Zhou, Junlong Du, Xiaohong Liu, Yue Fan, Qing Li, and Yuntao Du. Parameter-efficient fine-tuning for pre-trained vision models: A survey. *arXiv preprint arXiv:2402.02242*, 2024. [1](#)
- [62] Yi Xin, Siqi Luo, Xuyang Liu, Haodi Zhou, Xinyu Cheng, Christina E Lee, Junlong Du, Haozhe Wang, MingCai Chen, Ting Liu, et al. V-petl bench: A unified visual parameter-efficient transfer learning benchmark. In *NeurIPS*, pages 80522–80535, 2025. [1](#)
- [63] Chen Xu, Yuhan Zhu, Haocheng Shen, Boheng Chen, Yixuan Liao, Xiaoxin Chen, and Limin Wang. Progressive visual prompt learning with contrastive feature re-formation. *IJCV*, pages 1–16, 2024. [2](#)
- [64] Jiacheng Yang, Wai Keung Wong, Lunke Fei, Shuping Zhao, Jie Wen, and Shaohua Teng. Decoupling visual and identity features for adversarial palm-vein image attack. *Neural Networks*, 180:106693, 2024. [i](#)
- [65] Bruce XB Yu, Jianlong Chang, Haixin Wang, Lingbo Liu, Shijie Wang, Zhiyu Wang, Junfan Lin, Lingxi Xie, Haojie Li, Zhouchen Lin, et al. Visual tuning. *CSUR*, 56(12):1–38, 2024. [1](#)
- [66] Xiaohua Zhai, Joan Puigcerver, Alexander Kolesnikov, Pierre Ruysen, Carlos Riquelme, Mario Lucic, Josip Djolonga, Andre Susano Pinto, Maxim Neumann, Alexey Dosovitskiy, et al. A large-scale study of representation learning with the visual task adaptation benchmark. *arXiv preprint arXiv:1910.04867*, 2019. [5](#)
- [67] Yuanhan Zhang, Kaiyang Zhou, and Ziwei Liu. Neural prompt search. *IEEE TPAMI*, 2024. [5](#), [6](#), [vi](#)
- [68] Henry Hengyuan Zhao, Pichao Wang, Yuyang Zhao, Hao Luo, Fan Wang, and Mike Zheng Shou. Sct: A simple baseline for parameter-efficient fine-tuning via salient channels. *IJCV*, 132(3):731–749, 2024. [5](#)
- [69] Sixiao Zheng, Jiachen Lu, Hengshuang Zhao, Xiatian Zhu, Zekun Luo, Yabiao Wang, Yanwei Fu, Jianfeng Feng, Tao Xiang, Philip HS Torr, et al. Rethinking semantic segmentation from a sequence-to-sequence perspective with transformers. In *CVPR*, pages 6881–6890, 2021. [vi](#)
- [70] Bolei Zhou, Hang Zhao, Xavier Puig, Sanja Fidler, Adela Barriuso, and Antonio Torralba. Scene parsing through ade20k dataset. In *CVPR*, pages 633–641, 2017. [vi](#)
- [71] Nan Zhou, Jiaxin Chen, and Di Huang. ivpt: Improving task-relevant information sharing in visual prompt tuning by cross-layer dynamic connection. *arXiv preprint arXiv:2404.05207*, 2024. [2](#), [5](#), [6](#), [vi](#), [vii](#)

PRO-VPT: Distribution-Adaptive Visual Prompt Tuning via Prompt Relocation

Supplementary Material

This appendix presents further details and results that could not be included in the main paper due to space constraints. The content is organized as follows:

- § **A** provides detailed explanations of the related technical concepts.
- § **B** provides the detailed pseudo-code of PRO-VPT.
- § **C** presents the complete results of distribution adjustments and offers an in-depth analysis of the underlying nature of ADO, which motivates the nested optimization formulation.
- § **D** presents attempts at adding-based adjustments, which demonstrate significant instability.
- § **E** explains why our proposed PR strategy relocates only a single prompt for each iteration.
- § **F** details the derivation of the Taylor expansion for the idleness score.
- § **G** provides more details of implementation.
- § **H** presents complete results for VTAB-1k and FGVC as well as additional experimental results.
- § **I** presents additional visualizations and analyses.
- § **J** discusses the limitations of PRO-VPT and points out the potential direction for our future work.

A. Detailed Explanations of Technical Concepts

To help readers better understand the relevant technical concepts mentioned in this paper, we provide a detailed explanation of the related approaches as follows:

Vision Transformer. Given an input image \mathbf{x} , ViT [7, 26, 64] first divides it into n_e fixed-sized patches. Each patch is then embedded into d -dimensional latent space and combined with position encoding. The resulting set of patch embeddings is denoted as $\mathbf{E}_0 = \{\mathbf{e}_{0j} \in \mathbb{R}^d\}_{j=1}^{n_e}$. A learnable classification token \mathbf{x}_0 is then concatenated with these embeddings, forming the input sequence $[\mathbf{x}_0, \mathbf{E}_0]$. This sequence is then fed into a series of L Transformer blocks $\{B_i(\cdot)\}_{i=1}^L$ as follows:

$$[\mathbf{x}_i, \mathbf{E}_i] = B_i([\mathbf{x}_{i-1}, \mathbf{E}_{i-1}]), \quad i = 1, 2, \dots, L. \quad (\text{i})$$

Visual Prompt Tuning. Given a set of trainable prompt tokens \mathbf{P} and the prompted backbone $f_{\mathbf{P}}(\cdot)$, the overall objective of VPT [22] is to optimize these prompts for effectively adapting the PVM to downstream tasks:

$$\min_{\mathbf{P}} \mathbb{E}_{(\mathbf{x}, y) \in \mathcal{T}_{tr}} [\mathcal{L}(f_{\mathbf{P}}(\mathbf{x}), y)]. \quad (\text{ii})$$

This formulation specifically corresponds to Eq. (2).

Depending on how the prompt set \mathbf{P} is distributed across the Transformer blocks, the standard VPT [22] can be categorized into two variants, VPT-Shallow and VPT-Deep:

VPT-Shallow. The entire set of p prompts, $\mathbf{P} = \{\mathbf{p}_k \in \mathbb{R}^d\}_{k=1}^p$, is introduced merely in the first block. The shallow-prompted model is formulated as:

$$[\mathbf{x}_1, \mathbf{Z}_1, \mathbf{E}_1] = B_1([\mathbf{x}_0, \mathbf{P}, \mathbf{E}_0]), \quad (\text{iii})$$

$$[\mathbf{x}_i, \mathbf{Z}_i, \mathbf{E}_i] = B_i([\mathbf{x}_{i-1}, \mathbf{Z}_{i-1}, \mathbf{E}_{i-1}]), \quad i = 2, 3, \dots, L. \quad (\text{iv})$$

VPT-Deep. The prompt set \mathbf{P} is uniformly distributed across all blocks, where each block i is allocated a subset of m prompts, $\mathbf{P}_i = \{\mathbf{p}_{ik} \in \mathbb{R}^d\}_{k=1}^m$, with $\mathbf{P} = \bigcup_{i=1}^L \mathbf{P}_i$. The formulation of the deep-prompted model is as follows:

$$[\mathbf{x}_i, \cdot, \mathbf{E}_i] = B_i([\mathbf{x}_{i-1}, \mathbf{P}_{i-1}, \mathbf{E}_{i-1}]), \quad i = 1, 2, \dots, L. \quad (\text{v})$$

where ‘ \cdot ’ indicates that VPT-Deep does not preserve the output corresponding to the prompt tokens \mathbf{P}_{i-1} .

Proximal Policy Optimization. PPO [48] is a widely used RL algorithm that can be applied to both discrete and continuous action spaces. Specifically, PPO-Clip updates policies by solving the following optimization problem:

$$\theta_{k+1} = \arg \min_{\theta} \mathbb{E}_{s, a \sim \pi_{\theta_k}} [L(s, a, \theta_k, \theta)], \quad (\text{vi})$$

where π is the policy, θ is the policy parameters, and k is the k -th step. It typically takes multiple steps of SGD to optimize the clipped surrogate function $L(\cdot, \cdot, \cdot, \cdot)$:

$$L(s, a, \theta_k, \theta) = \min \left(\frac{\pi_{\theta}(a|s)}{\pi_{\theta_k}(a|s)} A^{\pi_{\theta_k}}(s, a), \text{clip} \left(\frac{\pi_{\theta}(a|s)}{\pi_{\theta_k}(a|s)}, 1 - \epsilon, 1 + \epsilon \right) A^{\pi_{\theta_k}}(s, a) \right), \quad (\text{vii})$$

where $A^{\pi_{\theta_k}}(s, a)$ is the advantage estimator, and ϵ is the clip hyper-parameter. The clipping mechanism constrains the new policy to stay close to the old one, preventing excessively large policy updates that could degrade performance [35, 48].

B. Pseudo-Code of PRO-VPT

We provide the detailed pseudo-code for PRO-VPT in Algo. i. Initially, it generates N prompts \mathbf{P} and distributes them to the PVM according to a uniform distribution \mathcal{D} (Line 1). In each epoch of PRO-VPT, it first calculates the estimated idleness scores $\{\hat{\mathcal{I}}_k\}_{k=1}^N$ using Eq. (6) (Line 3). If $\max \hat{\mathcal{I}}_k > 0$, the PR process is triggered. This process begins by pruning the prompt \mathbf{p}_{k^*} with the highest score $\hat{\mathcal{I}}_{k^*}$, thereby constructing an intermediate distribution \mathcal{D}^- (Line 5). The current state of the distribution s is then computed, followed by determining the action a^* based on PPO (Lines 6 and 7). Subsequently, the pruned prompt \mathbf{p}_{k^*} is allocated to the a^* -th block, resulting in a relocated distribution \mathcal{D}^+ (Line 8).

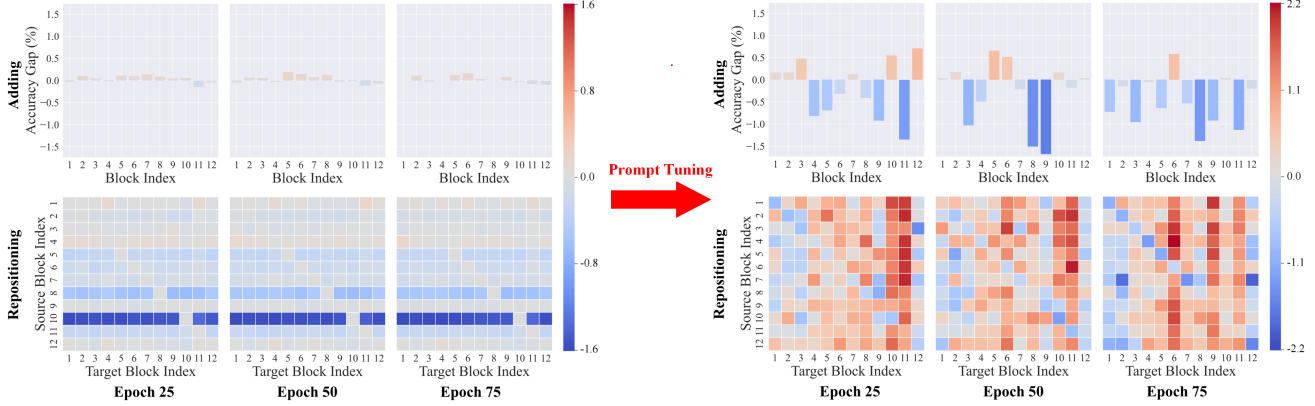


Figure i. **Detailed performance gaps from distribution adjustments** using prompts at epochs 25, 50, and 75, before and after prompt tuning. *Left*: Performance gaps from adjustments before prompt tuning. *Right*: Performance gaps from adjustments after prompt tuning. The effectiveness of distribution adjustments becomes apparent only after prompt tuning has been applied, and it also shifts with prompt updates.

Algorithm i: PRO-VPT

Input: pre-trained model f , number of epochs T , number of prompts N , learning rate η .

- 1 Initialize N prompts \mathbf{P} and distribute them to the model according to a uniform distribution \mathcal{D} .
 - 2 **for** $t = 0, \dots, T - 1$ **do**
 - 3 Compute idleness scores $\{\widehat{\mathcal{I}}_k\}_{k=1}^N$ by Eq. (6).
 - 4 **if** $\max \widehat{\mathcal{I}}_k > 0$ **then**
 - 5 **Prune** the negative prompt \mathbf{p}_{k^*} with the maximum idleness score $\widehat{\mathcal{I}}_{k^*}$ to form \mathcal{D}^- .
 - 6 Compute the current state s .
 - 7 Compute the action $a^* \leftarrow \text{PPO}(s)$.
 - 8 **Allocate** the idle prompt \mathbf{p}_{k^*} to the a^* -th block to form \mathcal{D}^+ .
 - 9 **end**
 - 10 Update the prompts as $\mathbf{P}' \leftarrow \mathbf{P} - \eta \cdot \mathbf{g}$.
 - 11 **if** $\max \widehat{\mathcal{I}}_k > 0$ **then**
 - 12 Compute the reward \hat{r} by Eq. (8).
 - 13 Update the policy networks within PPO based on \hat{r} .
 - 14 **end**
 - 15 **end**
-

After completing the PR process, the prompts are optimized to \mathbf{P}' (Line 10). Additionally, if the PR process is activated during the epoch, it is necessary to calculate the estimated reward \hat{r} using Eq. (8) and update the policy networks in PPO accordingly (Lines 12 and 13).

C. Comprehensive Analysis of the Underlying Nature behind ADO

Fig. i presents the complete results of Fig. 2. Specifically, we investigated the performance gaps from distribution adjustments applied to prompts at different epochs, both before

and after prompt tuning, on VTAB-1k *Natural* DTD using ViT-B/16. For the adding-based adjustment, we trained with a total of 59 prompts distributed uniformly across 12 Transformer blocks, resulting in one block containing 4 prompts while the others contained 5, then added a new prompt to the block with 4 prompts. For the repositioning-based adjustment, we trained with 60 prompts allocated uniformly, and then repositioned a single prompt. For fair comparisons, we averaged the results over five runs with different configurations, including variations in which block had the missing prompt as well as which specific prompt was repositioned.

The following provides a summary of the analysis and key findings presented in the main paper:

Finding 3. *The effectiveness of distribution adjustments becomes apparent only after prompt tuning, suggesting that these adjustments can only be properly evaluated after tuning, thereby forming a nested relationship between ADO and VPT.* Comparing the left and right parts of Fig. i, we find that adjusting the distribution without prompt tuning leads to negligible changes or even degrades performance. In contrast, implementing prompt tuning after adjusting the distribution leads to significant performance changes, with well-chosen adjustments leading to notable improvements (e.g., an increase of up to 2.2 pp achieved by repositioning just a single prompt). To this end, the proper workflow for ADO and VPT should be established as ‘distribution adjustment \rightarrow prompt tuning \rightarrow adjustment evaluation’, with prompt tuning nested within the distribution optimization process.

Finding 2. *Adjustments in prompt distribution are influenced by the updated prompts themselves, underscoring the necessity of an iterative process that continuously refines the distribution over prompt updates.* As demonstrated in the right portion of Fig. i, for prompts from epoch 25, we observe significant performance gains by adding a new prompt to the 10-th and 12-th blocks, as well as by repositioning one

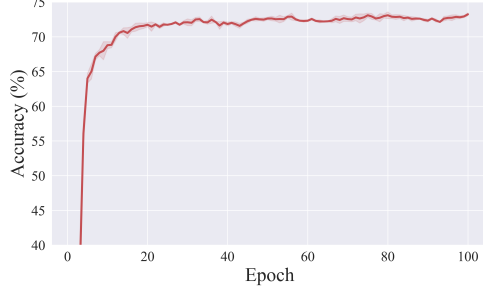


Figure ii. **Convergence curve across different prompt-tuning epochs**, which corresponds to Fig. i.

prompt to the 10-th and 11-th blocks. However, for prompts at epoch 75, the key improvements shifted to adding to the 6-th block and repositioning to the 6-th and 9-th blocks. To this end, the ADO-VPT co-design workflow should be established as an iterative process, which would be ‘distribution adjustment → prompt tuning → adjustment evaluation → new adjustment’.

Additionally, to validate that the performance improvements from applying both distribution adjustments and prompt tuning mainly result from the distribution adjustments rather than the tuning itself, we present the respective prompt tuning accuracy curve in Fig. ii. Clearly, the prompted model has already converged around epoch 20, with only slight performance fluctuations thereafter (less than 0.3 pp). This indicates that the performance differences observed in Fig. i (typically exceeding 0.3 pp) cannot be attributed solely to prompt tuning alone, but rather to the adjustments for the prompt distribution.

Building upon the underlying nature described in **Findings 2** and **3**, a proper workflow for ADO and VPT should be structured as an iterative nested process. Specifically, in each iteration, the process first adjusts the distribution to construct \mathcal{D}^* , then tunes the visual prompts to obtain \mathbf{P}^* . Based on \mathcal{D}^* and \mathbf{P}^* , the effectiveness of the distribution adjustment is evaluated at the end of each iteration, marking the completion of the current cycle and the beginning of the next. Fig. iii illustrates this co-design workflow for ADO and VPT. Formally, it can be expressed as a nested optimization problem as follows:

$$\mathcal{D}^* = \arg \min_{\mathcal{D}} \mathbb{E}_{(\mathbf{x}, y) \in \mathcal{T}_{tr}} [\mathcal{L}(f_{\mathbf{P}^*, \mathcal{D}}(\mathbf{x}), y)], \quad (\text{viii})$$

$$\mathbf{P}^* = \arg \min_{\mathbf{P}} \mathbb{E}_{(\mathbf{x}, y) \in \mathcal{T}_{tr}} [\mathcal{L}(f_{\mathbf{P}, \mathcal{D}^*}(\mathbf{x}), y)], \quad (\text{ix})$$

where the notations \mathbf{P}^* and \mathcal{D}^* correspond to those depicted in Fig. iii.

Overall, the ADO problem is naturally formulated as a nested problem, grounded in its underlying nature. This formulation is applicable to various distribution adjustment strategies (*e.g.*, adding, repositioning, or even pruning) as

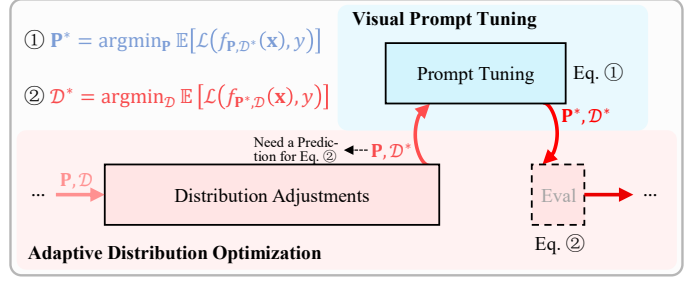


Figure iii. **Proper workflow of ADO-VPT co-design framework**. It is framed as an iterative process, with the VPT process nested within the ADO process.

well as different discrete optimization methods (*e.g.*, evolutionary algorithms and reinforcement learning). Notably, since distribution adjustments can only be evaluated at the end, a prediction for Eq. viii is necessary for selecting an appropriate adjustment. To this end, it is natural to frame ADO as a RL problem, where the reward is predicted to determine the next action, and the effectiveness of that action is evaluated afterward.

D. Inferior Performance of Adding-based Adjustments

Following the nested optimization framework described in Eqs. (viii) and (ix), we have also attempted to develop an adding-based strategy for ADO. Given that framing the ADO objective as a RL problem is a suitable choice (refer to § 3.3 and § C), we also address the adding-based ADO by leveraging RL, with the components of the Markov decision process specified as follows:

1) *State*. We utilize the current prompt distribution as the state, denoted as $s = \mathcal{D}$. After adding a new prompt and performing prompt tuning, the state transitions to s' .

2) *Action*. Unlike prompt repositioning, which considers L^2 possible block arrangements, the adding-based ADO involves only L potential adding operations. As a result, the adding-based ADO does not require decomposition for RL,

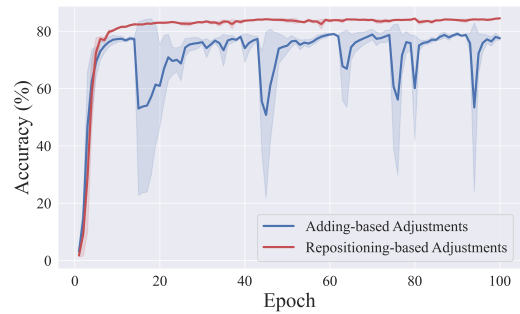


Figure iv. **Convergence curves comparing adding-based and repositioning-based strategies**. The adding-based strategy exhibits significantly less stability.

and the action is straightforwardly represented as $a \in [L]$.

3) *Reward*. Similar to the PR strategy, the reward is formulated based on Eq. (viii) as $r = \Delta\mathcal{L}(f_{\mathbf{P},\mathcal{D}}, f_{\mathbf{P}',\mathcal{D}'})$, where \mathcal{D}' denotes the updated prompt distribution after adding and \mathbf{P}' represents the tuned prompts.

Similarly, we employ PPO for this RL problem to tackle the adding-based ADO objective, while adopting the overall framework illustrated in Fig. iii.

Fig. iv illustrates the performance comparison between the adding-based strategy and repositioning-based strategy (PRO-VPT) on the VTAB-1k *Natural* Cifar100 dataset. It can be clearly observed that the adding-based strategy is significantly less stable and underperforms compared to the repositioning-based approach. We attribute this discrepancy to the undertraining of newly added prompts and potential conflicts with existing ones. Consequently, our work focuses on developing the repositioning-based strategy for ADO.

E. Relocating One Prompt for Each Iteration

Here, we explain why we restrict the relocation process to operate on only a single prompt for each iteration. Since we frame the allocation step as a RL problem, we need to evaluate the effectiveness of each allocation decision for relocated prompts. Relocating more than one prompt simultaneously would necessitate multiple reward evaluations, substantially increasing task complexity and computational overhead. Therefore, we designed to relocate only one prompt per iteration to maintain simplicity and efficiency in the allocation process.

F. Derivation of the Taylor Expansion for the Idleness Score

Based on the pruning objective in Eq. (3), the original idleness score is defined as:

$$\mathcal{I}_k = \Delta\mathcal{L}(f_{\mathbf{P},\mathcal{D}}, f_{\mathbf{P},\mathcal{D}|d_k=0}), \quad (\text{x})$$

where $d_k = 0$ indicates that the k -th prompt is pruned. Equivalently, this equation can be expressed as:

$$\mathcal{I}_k = \Delta\mathcal{L}(f_{\mathbf{P},\mathcal{D}}, f_{\mathbf{P}|\mathbf{p}_k=\mathbf{0},\mathcal{D}}), \quad (\text{xi})$$

where $\mathbf{p}_k = \mathbf{0}$ represents that the k -th prompt is a zero vector.

Let $p_{kj} \in \mathbf{p}_k$ denote as the prompt parameter. The difference in losses with and without the prompt parameter, *i.e.*, the idleness score of p_{kj} , is given by:

$$\mathcal{I}_{kj} = \Delta\mathcal{L}(f_{\mathbf{P},\mathcal{D}}, f_{\mathbf{P}|p_{kj}=0,\mathcal{D}}). \quad (\text{xii})$$

Considering the entire prompt set as a concatenated vector $\mathbf{P} = \{p_{00}, p_{01}, \dots, p_{Nd}\}$, we are able to approximate \mathcal{I}_{kj} in

Table i. **Hyper-parameters for VPT and PRO-VPT.**

	VPT	PRO-VPT
Batch size	64 ($p \geq 100$), 128 ($p < 100$)	64
Learning rate schedule	cosine decay	-
Optimizer	SGD	
Optimizer momentum	0.9	
<i>base_lr</i> range	{50., 25., 10., 5., 2.5, 1., 0.5, 0.25, 0.1, 0.05}	
Weight decay range	{0.01, 0.001, 0.0001, 0.0}	
Drop rate	0.1	
Total epochs	100	

the vicinity of \mathbf{P} by its first-order Taylor expansion:

$$\begin{aligned} \widehat{\mathcal{I}}_{kj} &\approx \mathbf{g}^T (\mathbf{P} - \mathbf{P}|_{p_{kj}=0}) \\ &\approx g_{kj} p_{kj}, \end{aligned} \quad (\text{xiii})$$

where $g_{kj} = \frac{\nabla \mathcal{L}}{\nabla p_{kj}}$ represents the element of the gradient \mathbf{g} .

For the idleness score of a prompt $\mathbf{p}_k = \{p_{kj}\}_{j=1}^d$, we can approximate it by summing the score of its individual parameters, as follows:

$$\widehat{\mathcal{I}}_k \approx \sum_{j=1}^d g_{kj} p_{kj} \approx \mathbf{g}_k^T \mathbf{p}_k. \quad (\text{xiv})$$

To this end, we are able to efficiently approximate the idleness scores $\{\mathcal{I}_k\}_{k=1}^N$ by a single backpropagation pass, thereby avoiding the need to evaluate the idleness scores of all N prompts individually.

G. More Implementation Details

Data Augmentation. Apart from data normalization, we resize the input images to 224×224 pixels for VTAB-1k and apply a randomly resize crop to 224×224 pixels and horizontal flipping for FGVC, as outlined in [13, 22, 51, 59].

Training Hyper-Parameters. Specific to training hyper-parameters, we largely adopt the same settings as depicted in VPT [22]. Tab. i summarizes the hyper-parameter configurations comparing the experiments of VPT and our approach. Following [13, 22], we conduct a grid search on the validation set of each task to determine the optimal learning rate and weight decay; the learning rate is set as $base_lr \times b/256$, where b denotes the batch size and $base_lr$ is selected from the range specified in Tab. i. Notably, PRO-VPT does not require specific-designed large learning rates as in [22]. For all experiments conducted with our implementation, the results are averaged over three random seeds.

PPO Hyper-Parameters. We also detail the hyper-parameters of our PPO implementation for reproducibility. Both the actor and critic networks are two-layer MLPs with 64 hidden units per layer. The total number of parameters of the two policy networks is precisely 0.0136M. The learning rates are 0.0003 for the actor and 0.001 for the critic. Additionally, we set the discount factor to 1 and the clipping factor to 0.2.

Table ii. Specifications of the VTAB-1k datasets.

Group	Task	#Classes	Splits		
			Train	Val	Test
Natural	CIFAR-100	100			10 000
	Caltech-101	102			6 084
	DTD	47			1 880
	Oxford Flowers	102	800	200	6 149
	Pets	37			3 669
	SVHN	10			26 032
	Sun397	397			21 750
Specialized	Patch Camelyon	2			32 768
	EuroSAT	10	800	200	5 400
	RESISC45	45			6 300
	Diabetic Retinopathy	5			42 670
Structured	CLEVR-Count	8			15 000
	CLEVR-Distance	6			15 000
	DMLab	6			22 735
	KITTI-Distance	4	800	200	711
	dSprites-Location	16			73 728
	dSprites-Orientation	16			73 728
	smallNORB-Azimuth	18			12 150
	smallNORB-Elevation	9			12 150

Datasets and Pre-Trained Backbones Specifications.

Tabs. ii and iii present the statistics of each task in VTAB-1k and FGVC *w.r.t.* the number of classes and the number of images in the train, validation, and test splits. The tables are largely “borrowed” from [51]. Moreover, Tab. iv provides the details of the pre-trained backbones used in this paper, which is largely “borrowed” from [22].

Reproducibility. PRO-VPT is implemented in Pytorch and timm. Experiments are conducted on NVIDIA A30-24GB GPUs. To guarantee reproducibility, our full implementation will be publicly released.

H. More Experimental Results

Complete Results for VTAB-1k. Tab. v presents comprehensive results for VTAB-1k, using both ImageNet and Inception normalizations. Although several of the best pre-task results from other PEFT methods differ and exceed those listed in Tab. 1, PRO-VPT remains highly competitive, achieving a state-of-the-art average accuracy of 78.0% among all evaluated methods.

Fig. v illustrates a comparison of prompt-based methods, including the previous state-of-the-art (iVPT), the baseline (VPT), and our proposal (PRO-VPT). All scores were normalized by $x_{norm} = x - x_{mean}$. It is evident that PRO-VPT outperforms both current leading methods, establishing a new state-of-the-art performance for prompt-based techniques.

Complete Results for FGVC. Tab. vi presents comprehensive results for FGVC, utilizing both ImageNet and Inception normalizations. The best pre-task results remain consistent with those in Tab. 2, and PRO-VPT demonstrates superior performance on large-scale fine-grained datasets.

Table iii. Specifications of the FGVC datasets. For datasets marked with *, we follow [51] to randomly sample train and validation splits since validation sets are not available from the original datasets.

Dataset	#Classes	Splits		
		Train	Val	Test
CUB-200-2011* [56]	200	5 394	600	5 794
NABirds* [55]	555	21 536	2 393	6 084
Oxford Flowers [42]	102	1 020	1 020	6 149
Stanford Dogs* [6]	120	10 800	1 200	8 580
Stanford Cars* [10]	196	7 329	815	8 041

Table iv. Specifications of the pre-trained backbones.

Backbone	Pre-trained Strategy	Pre-trained Dataset	Param (M)	Feature dim d	Pre-trained Model
ViT-B/16			85	768	checkpoint
ViT-L/16	Supervised	ImageNet-21k	307	1024	checkpoint
ViT-H/14			630	1280	checkpoint
Swin-B	Supervised	ImageNet-21k	88	1024	checkpoint
ViT-B/16	MAE				checkpoint
ViT-B/16	MoCo-v3	ImageNet-1k	85	768	checkpoint

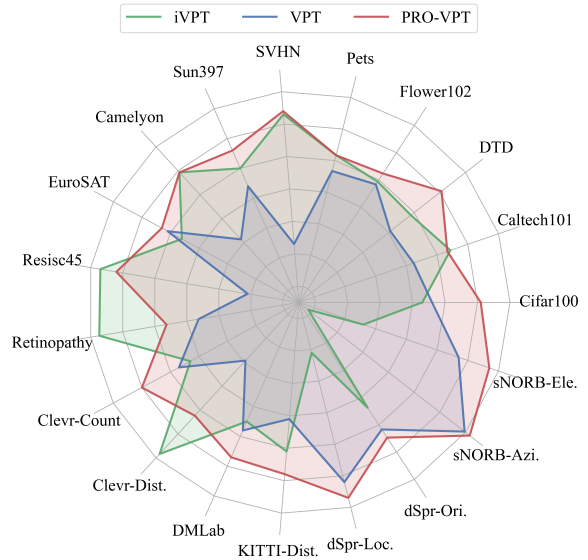


Figure v. Comparison of prior state-of-the-art (iVPT), baseline (VPT), and our method (PRO-VPT). Our approach subsumes two representative methods.

Generalizability Study on Detection and Segmentation Tasks.

We also conduct experiments on a broader range of downstream tasks, including object detection, instance segmentation, and semantic segmentation. Specifically, we evaluate object detection and instance segmentation performance on the COCO dataset [36], using Mask R-CNN [17] with a Swin-T backbone pre-trained on ImageNet-1k. For the

Table v. **Comprehensive results on the VTAB-1k datasets.** Performance results are reported using both ImageNet normalization (◦) or Inception normalization (●), presented in % after a complete training schedule with ViT-B/16 supervised pre-trained on ImageNet-21k. The best results of prompt-based methods and other PEFT approaches are highlighted in **bold**. ‡: Early-stopping based on the test set. †: Lack of complete code or hyperparameter configurations for the method, hence results are reported as presented in the original paper. ¹Average across the average accuracies of the VTAB-1k groups, following previous work.

	Param (M)	Natural							Specialized				Structured						Global Avg. ¹					
		Cifar100	Caltech101	DTD	Flower102	Pets	SVHN	Suns397	Group Avg.	Camelyon	EuroSAT	Resisc45	Retinopathy	Group Avg.	Clevr-Count	Clevr-Dist.	DMLab	KITTI-Dist.		dSpr-Loc.	dSpr-Ori.	sNORB-Azi.	sNORB-Ele.	Group Avg.
Full ◦	85.8	68.9	87.7	64.3	97.2	86.9	87.4	38.8	75.9	79.7	95.7	84.2	73.9	83.4	56.3	58.6	41.7	65.5	57.5	46.7	25.7	29.1	47.6	69.0
Full ●	85.8	73.2	92.6	70.4	97.9	86.2	90.6	39.6	78.6	87.1	96.6	87.5	74.0	86.3	66.6	61.0	49.8	79.7	82.6	51.9	33.5	37.0	57.8	74.2
Linear ◦	0.04	63.4	85.0	63.2	97.0	86.3	36.6	51.0	68.9	78.5	87.5	68.6	74.0	77.2	34.3	30.6	33.2	55.4	12.5	20.0	9.6	19.2	26.9	57.7
Linear ●	0.04	78.1	88.1	69.0	99.1	90.0	36.0	56.9	73.9	79.8	90.7	73.7	73.7	79.5	32.4	30.5	35.9	61.9	11.2	26.2	14.3	24.5	29.6	61.0
LoRA ● [20]	0.29	83.0	91.7	71.6	99.2	90.9	83.8	56.7	82.4	86.2	95.7	83.5	71.9	84.3	77.7	62.3	49.0	80.2	82.2	51.7	31.0	47.0	60.1	75.6
FacT-TK _s ◦ [23]	0.05	70.3	88.7	69.8	99.0	90.4	84.2	53.5	79.4	82.8	95.6	82.8	75.7	84.2	81.1	68.0	48.0	80.5	74.6	44.0	29.2	41.1	58.3	74.0
FacT-TK _s ● [23]	0.05	74.9	92.7	73.7	99.1	91.3	85.5	57.7	82.1	86.8	94.9	84.1	70.9	84.2	81.9	64.1	49.2	77.2	83.8	53.1	28.2	44.7	60.3	75.5
FacT-TK _{≤32} ◦ [23]	0.10	70.6	90.6	70.8	99.1	90.7	88.6	54.1	80.6	84.8	96.2	84.5	75.7	85.3	82.6	68.2	49.8	80.7	80.8	47.4	33.2	43.0	60.7	75.6
FacT-TK _{≤32} ● [23]	0.10	74.6	93.7	73.6	99.3	90.6	88.7	57.5	82.6	87.6	95.4	85.5	70.4	84.7	84.3	62.6	51.9	79.2	85.5	52.0	36.4	46.6	62.3	76.5
Consolidator † [15]	0.30	74.2	90.9	73.9	99.4	91.6	91.5	55.5	82.4	86.9	95.7	86.6	75.9	86.3	81.2	68.2	51.6	83.5	79.8	52.3	31.9	38.5	60.9	76.5
SSF ‡ ◦ [34]	0.24	69.0	92.6	75.1	99.4	91.8	90.2	52.9	81.6	87.4	95.9	87.4	75.5	86.6	75.9	62.3	53.3	80.6	77.3	54.9	29.5	37.9	59.0	75.7
SSF ‡ ● [34]	0.24	61.9	92.3	73.4	99.4	92.0	90.8	52.0	80.3	86.5	95.8	87.5	72.8	85.7	77.4	57.6	53.4	77.0	78.2	54.3	30.3	36.1	58.0	74.6
SPT-Adapter ‡ ◦ [16]	0.23	72.9	93.2	72.5	99.3	91.4	84.6	55.2	81.3	85.3	96.0	84.3	75.5	85.3	82.2	68.0	49.3	80.0	82.4	51.9	31.7	41.2	60.8	75.8
SPT-Adapter ‡ ● [16]	0.22	74.7	94.1	73.0	99.1	91.2	84.5	57.5	82.0	85.7	94.9	85.7	70.2	84.1	81.3	63.2	49.1	80.7	83.5	52.0	26.4	41.5	59.7	75.3
SPT-Adapter ‡ ◦ [16]	0.43	72.9	93.2	72.5	99.3	91.4	88.8	55.8	82.0	86.2	96.1	85.5	75.5	85.8	83.0	68.0	51.9	81.2	82.4	51.9	31.7	41.2	61.4	76.4
SPT-Adapter ‡ ● [16]	0.43	74.9	93.2	71.6	99.2	91.1	87.9	57.2	82.2	87.0	95.4	86.5	72.4	85.3	81.1	63.2	50.3	80.2	84.4	51.4	31.5	42.2	60.5	76.0
Adapter+r=16 ● [51]	0.35	83.7	94.2	71.5	99.3	90.6	88.2	55.8	83.3	87.5	97.0	87.4	72.9	86.2	82.9	60.9	53.7	80.8	88.4	55.2	37.3	46.9	63.3	77.6
Prompt-based Methods:																								
VPT-Deep ◦ [22]	0.60	78.8	90.8	65.8	98.0	88.3	78.1	49.6	78.5	81.8	96.1	83.4	68.4	82.4	68.5	60.0	46.5	72.8	73.6	47.9	32.9	37.8	55.0	72.0
VPT-Deep ● [22]	0.60	83.0	93.0	71.2	99.0	91.3	84.1	56.0	82.5	84.9	96.6	82.5	74.5	84.6	77.5	58.7	49.7	79.6	86.2	56.1	37.9	50.7	62.1	76.4
NOAH ‡ ◦ [67]	0.43	69.6	92.7	70.2	99.1	90.4	86.1	53.7	80.2	84.4	95.4	83.9	75.8	84.9	82.8	68.9	49.9	81.7	81.8	48.3	32.8	44.2	61.3	75.5
SPT-Adapter † [58]	0.22	79.3	92.6	73.2	99.5	91.0	89.1	51.2	82.3	85.4	96.8	84.9	74.8	85.5	70.3	64.8	54.2	75.2	79.3	49.5	36.5	41.5	58.9	75.6
iVPT † [71]	0.60	82.7	94.2	72.0	99.1	91.8	88.1	56.6	83.5	87.7	96.1	87.1	77.6	87.1	77.1	62.6	49.4	80.6	82.1	55.3	31.8	47.6	60.8	77.1
PRO-VPT (ours)	0.61	84.5	94.1	73.2	99.4	91.8	88.2	57.2	84.1	87.7	96.8	86.6	75.5	86.7	78.8	61.0	50.6	81.3	86.7	56.4	38.1	51.7	63.1	78.0

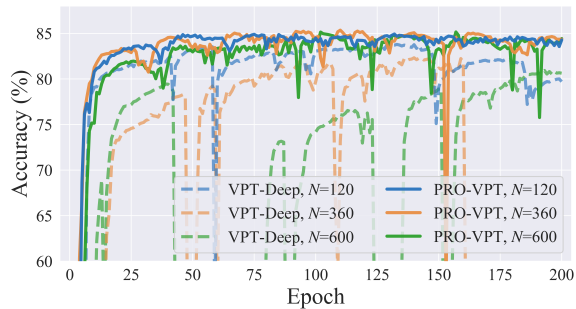


Figure vi. **Convergence curves comparing VPT and PRO-VPT** with varying numbers of prompts. PRO-VPT exhibits superior robustness.

semantic segmentation task, we use the ADE20k dataset [70] and adopt SETR-PUP [69] with a ViT-B/16 backbone pre-trained on ImageNet-21k. As shown in Tab. vii, the results demonstrate that PRO-VPT consistently outperforms VPT across both detection and segmentation tasks, highlighting its superior generalizability.

Convergence Curves with Different Prompt Numbers.

Fig. vi illustrates the convergence curves under varying total numbers of prompts on VTAB-1k Natural Cifar100, with training extended to 200 epochs. Notably, VPT exhibits high sensitivity to the number of prompts, as discussed in [21, 58].

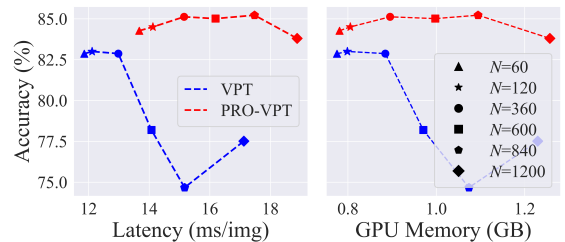


Figure vii. **Cost comparisons** with different prompt numbers. We report the latency (ms/img) and the GPU memory usage (GB). The increased training time associated with PRO-VPT is justified by the considerable enhancements in both performance and robustness.

An improper prompt number can lead to significant instability during convergence and result in inferior performance. In contrast, PRO-VPT demonstrates remarkable robustness to variations in prompt quantity. Although it is slightly affected during the initial convergence phase, our method ultimately converges to consistent performance. This suggests that learning the optimal distribution enables a more nuanced calibration of tuning intensity at each block, thereby enhancing robustness.

Cost Analysis. As detailed in § 3, estimating the expected objectives effectively avoids additional computation, thereby

Table vi. **Comprehensive results on the FGVC datasets.** Performance results are reported as the highest of ImageNet normalization (\circ) or Inception normalization (\bullet), presented in % after a complete training schedule with ViT-B/16 supervised pre-trained on ImageNet-21k. The best results of prompt-based methods and other PEFT approaches are highlighted in **bold**. †: Lack of complete code or hyperparameter configurations for the method, hence results are reported as presented in the original paper.

	Param (M)	CUB200	NABirds	Oxford Flowers	Stanford Dogs	Stanford Cars	Global Avg.
Full \circ	86.0	87.3	82.7	98.8	89.4	84.5	88.5
Full \bullet	86.0	88.0	81.5	99.2	85.6	90.6	89.0
Linear \circ	0.18	85.3	75.9	97.9	86.2	51.3	79.3
Linear \bullet	0.18	88.9	81.8	99.5	92.6	52.8	83.1
SSF \circ [34]	0.39	89.5	85.7	99.6	89.6	89.2	90.7
SSF \bullet [34]	0.39	88.9	85.0	99.6	88.9	88.9	90.3
SPT-Adapter † [16]	0.40	89.1	83.3	99.2	91.1	86.2	89.8
SPT-LoRA † [16]	0.52	88.6	83.4	99.5	91.4	87.3	90.1
Adapter+ \bullet [51]	0.34	90.4	85.0	99.7	92.6	89.1	91.4
Prompt-based Methods:							
VPT-Deep \circ [22]	0.85	88.5	84.2	99.0	90.2	83.6	89.1
VPT-Deep \bullet [22]	0.85	90.1	83.3	99.6	90.3	85.0	89.7
SPT-Deep † [58]	0.36	90.6	87.6	99.8	89.8	89.2	91.4
iVPT † [71]	0.41	89.1	84.5	99.5	90.8	85.6	89.9
PRO-VPT (ours)	0.86	90.6	86.7	99.7	91.8	89.6	91.7

Table vii. **Generalizability study on detection and segmentation tasks.** Results are presented on two instances: COCO val2017 and ADE20k.

	COCO with Mask R-CNN						ADE20k with SETR	
	AP ^b	AP ₅₀ ^b	AP ₇₅ ^b	AP ^m	AP ₅₀ ^m	AP ₇₅ ^m	mIoU-SS	mIoU-MS
VPT-Deep	33.8	57.6	35.3	32.5	54.5	33.9	39.1	40.1
PRO-VPT	34.6	58.6	36.1	33.4	55.5	34.7	40.0	41.0

¹ AP^b and AP^m are the average precision for objective detection and instance segmentation.

² mIoU-SS and mIoU-MS are single- and multi-scale inference of semantic segmentation.

significantly enhancing the efficiency of our method. In particular, the extra training cost of our method primarily stems from the computation of policy networks in PPO. However, since the policy networks are merely lightweight MLPs, this additional cost is relatively low. Specifically on VTAB-1k, the average latency for VPT and PRO-VPT is 13.37 ms/img and 15.55 ms/img (**1.16** \times). Furthermore, we evaluate latency and GPU usage with varying prompt numbers on VTAB-1k *Natural* Cifar100 in Fig. vii. Although PRO-VPT does introduce some extra training time, the performance and robustness improvements justify this cost, and the increase in GPU memory usage is marginal.

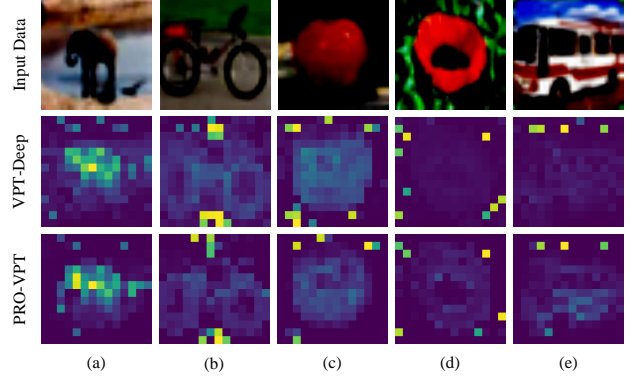


Figure viii. **Visualization of attention maps.** PRO-VPT exhibits more focused and precise attention with fewer artifacts.

I. Visualization and Analysis

Attention Maps. We visualize the attention maps between [CLS] and image patches on VTAB-1k *Natural* Cifar100. As shown in Figs. viii(a)-(c), while VPT successfully focuses on the object, its attention exhibits significant artifacts [4] and, more critically, remains scattered. For example, in Fig. viii(a), VPT shows certain attention on the lake, which is actually part of the background. In contrast, PRO-VPT demonstrates more focused and accurate attention with fewer artifacts. Furthermore, as illustrated in Figs. viii(d) and (e), VPT appears to struggle with effectively concentrating on the object, whereas PRO-VPT maintains its ability to focus on the object.

Learned Distributions and Accuracy Curves. Fig. ix illustrates the learned distributions in PRO-VPT as well as the accuracy curves in comparison to VPT, based on 100 training epochs. Empirical results from more datasets further reinforce that the prompting importance for each block is inherently task-dependent. Moreover, the comparison of accuracy curves between PRO-VPT and VPT, particularly on the SVHN, Camelyon, and Resisc45 datasets, reveals that PRO-VPT still exhibits an upward trend in accuracy during the late training stages. This highlights the effectiveness of learning the optimal distribution for visual prompts, which unlocks their full potential and maximizes downstream performance.

J. Limitation and Future Work

Despite demonstrating promising performance and enhanced robustness, our approach still has certain limitations. First, as noted in [21, 58], prompt-based methods are significantly sensitive to the total number of prompts. Although our method improves robustness and mitigates this issue to some extent (refer to § 4.5), there is still room for further refinement. In particular, while PRO-VPT maintains robust performance within a certain range (*e.g.*, 120-600 initialized

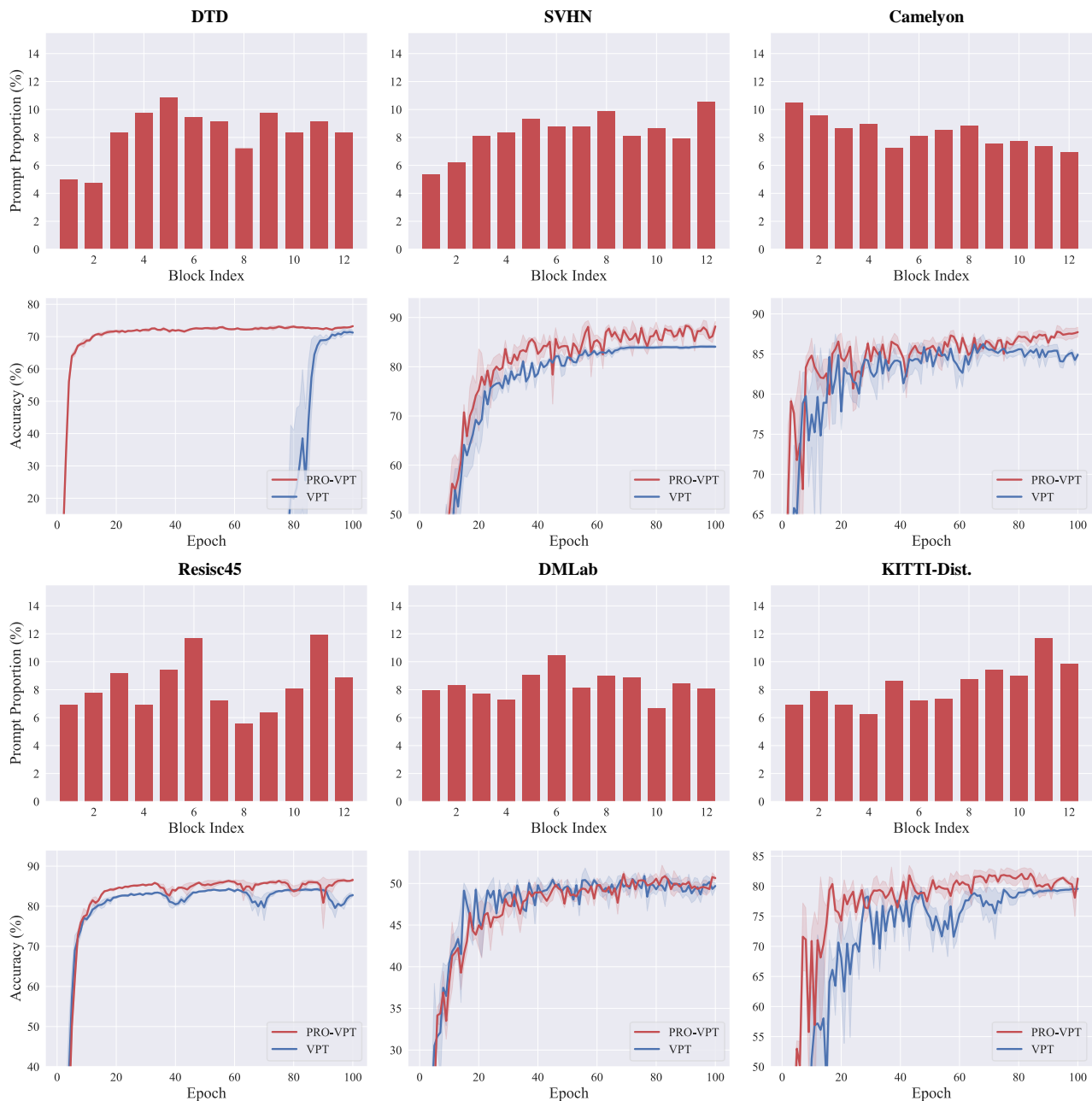


Figure ix. **Visualization of the prompt distributions learned by PRO-VPT and the accuracy curves compared to VPT on the VTAB-1k datasets: *Natural* DTD, SVHN; *Specialized* Camelyon, Resisc45; and *Structured* DMLab, KITTI-Dist.**

prompts as in Fig. vi), its performance still deteriorates when the number of prompts deviates significantly from the optimal value. Consequently, our method still employs the optimal total number of prompts per task from [22], resulting in relatively high parameter counts as in VPT. Second, the constraint of relocating one prompt per iteration (see § E) restricts our method to relocating only limited prompts within certain epochs. This particularly affects tasks requiring high prompt numbers, hindering PRO-VPT’s ability to

learn optimal distributions. For instance, the changes from initial uniform to learned prompt distributions are relatively less pronounced for Camelyon and DMLab as shown in Fig. ix, which require 100 initialized prompts per block. Nevertheless, it is worth noting that PRO-VPT still delivers considerable performance enhancements on these datasets. Addressing these limitations would further enhance the efficiency and applicability of our approach in diverse downstream tasks.

Moreover, while this paper focuses on calibrating the distribution of prompts, the PRO-VPT framework is applicable to most block-wise PEFT approaches, *e.g.*, adjusting the pre-block dimension of subspaces (*i.e.*, the rank distribution) in adapter-based methods. An essential future direction deserving of further investigation is integrating our approach with other PEFT methods, developing a universal framework for fine-grained robust PEFT.